JEM Journal of Experimental Medicine

ARTICLE

Transcription factor Zhx2 restricts NK cell maturation and suppresses their antitumor immunity

Siyu Tan[1], Xiaowei Guo[1], Mengzhen Li[1], Tixiao Wang[1], Zehua Wang[1], Chunyang Li[4], Zhuanchang Wu[1], Nailin Li[5], Lifen Gao[1,3], Xiaohong Liang[1,3], and Chunhong Ma[1,2,3]

The maturation and functional competence of natural killer (NK) cells is a tightly controlled process that relies on transcription factors (TFs). Here, we identify transcriptional repressor zinc fingers and homeoboxes 2 (Zhx2) as a novel regulator that restricts NK cell maturation and function. Mice with *Zhx2* conditional deletion in NK cells (*Zhx2*$^{\Delta/\Delta}$) showed accumulation of matured NK cells. Loss of *Zhx2* enhanced NK cell survival and NK cell response to IL-15. Transcriptomic analysis revealed *Zeb2*, a key TF in NK cell terminal maturation, as a direct downstream target of Zhx2. Therapeutically, transfer of *Zhx2*-deficient NK cells resulted in inhibition of tumor growth and metastasis in different murine models. Our findings collectively unmask a previously unrecognized role of Zhx2 as a novel negative regulator in NK cell maturation and highlight its therapeutic potential as a promising strategy to enhance NK cell–mediated tumor surveillance.

Introduction

Natural killer (NK) cells contribute to the host's first line of tumor immunosurveillance with the ability to identify and eliminate transformed cells through the release of cytotoxic granules containing perforin and granzymes (Huntington et al., 2007b; Vivier et al., 2008). Harnessing NK cell effector function represents a critical immunotherapeutic approach to cancer (Guillerey et al., 2016). Although NK cells are set up throughout development to be potent killers, their roles can be subverted at the tumor site (Mamessier et al., 2011; Sconocchia et al., 2012). Tumor-infiltrating NK (TINK) cells frequently exhibit a dysfunctional phenotype, express decreased levels of activating receptors and increased levels of inhibitory receptors, produce lesser amounts of cytokines such as IFN-γ, and exert lower cytotoxicity. Both animal data and clinical evidence suggest the loss of functional NK cells and the accumulation of inactive and immature NK cells in the tumor microenvironment (Jacobs et al., 2001; Platonova et al., 2011; Richards et al., 2006). A better understanding of the molecular regulatory mechanisms that control NK cell maturation and survival is crucial for the development of NK cell–based immunotherapies.

NK cells develop mainly in the bone marrow (BM). After the acquisition of the IL-15 receptor β chain (CD122), followed by the expression of NK1.1, NK cells continue a late maturation program that can be further classified based on the surface expression of CD11b and CD27: CD11b$^-$CD27$^+$, CD11b$^+$CD27$^+$, and CD11b$^+$CD27$^-$ (Chiossone et al., 2009; Kim et al., 2002). During maturation, NK cells gradually increase CD11b expression, decrease CD27 expression, maintain a balance between the expression of activating and inhibitory receptors, progressively increase their cytotoxic capacity but decrease their potential for homeostatic expansion, and become prone to apoptosis (White et al., 2017). NK cell development and functional maturation are triggered by plenty of extracellular signals (i.e., cytokines), among which IL-15 is critical for both NK cell lineage commitment and terminal maturation (Huntington et al., 2007a). In addition, NK cell development is dictated by a series of transcription factors (TFs) that promote the expression of genes coding for effector molecules and surface markers of maturation (Brillantes and Beaulieu, 2019). For instance, *Id2* (Constantinides et al., 2014; Delconte et al., 2016), *STAT5* (Marçais et al., 2014; Vargas-Hernández et al., 2020), *Tox* (Vong et al., 2014), *Ets1*

[1]Key Laboratory for Experimental Teratology of the Ministry of Education, Key Laboratory of Infection and Immunity of Shandong Province, and Department of Immunology, School of Basic Medical Sciences, Cheeloo Medical College of Shandong University, Jinan, Shandong, China; [2]Advanced Medical Research Institute, Shandong University, Jinan, Shandong, China; [3]Collaborative Innovation Center of Technology and Equipment for Biological Diagnosis and Therapy in Universities of Shandong, Jinan, Shandong, China; [4]Key Laboratory for Experimental Teratology of the Ministry of Education, Department of Histology and Embryology, School of Basic Medical Sciences, Cheeloo Medical College of Shandong University, Jinan, Shandong, China; [5]Clinical Pharmacology Group, Department of Medicine, Solna, Karolinska Institutet, Stockholm, Sweden.

Correspondence to Chunhong Ma: machunhong@sdu.edu.cn.

(Barton et al., 1998; Taveirne et al., 2020), and *Nfil3* (Seillet et al., 2014) regulate early stages of NK development, whereas concerted actions of *T-bet* and *Zeb2* determine terminal NK cell maturation and survival (Gordon et al., 2012; van Helden et al., 2015). Although huge advances have been achieved in transcriptional regulation of NK development, negative regulators in the process of NK cell maturation are still largely unknown.

Zinc fingers and homeoboxes 2 (Zhx2), one member of the ZHX family, is identified as a ubiquitous transcriptional repressor (Liu et al., 2015). Zhx2 has attracted considerable attention due to its involvement in tumorigenesis, cell differentiation, and metabolism-related diseases (Wu et al., 2020b; You et al., 2020; Yue et al., 2012), whereas its function in the immune system is mostly overlooked. Zhx2 is abundantly expressed in the thymus and spleen and has been reported to play a role in B cell development and macrophage polarization (Nagel et al., 2015; Wang et al., 2020). By manipulating macrophage activation and differentiation, Zhx2 participates in inflammation-related diseases such as atherosclerosis and sepsis (Erbilgin et al., 2018; Wang et al., 2020). These findings indicate Zhx2 as a potentially interesting gene in immune cell differentiation. However, its function in NK cells is unclear.

Here, we identified Zhx2 as a novel regulator of NK cells that restricts NK cell maturation, survival programs, and effector functions. Mechanically, Zhx2 lowered NK cell responses to IL-15 and transcriptionally repressed *Zeb2* expression. Deletion of *Zhx2* in NK cells markedly enhanced the formation of mature NK cells and promoted curative antitumor immunity of NK cell adoptive immunotherapy. These data provide new insight into the regulatory mechanisms of NK cell maturation and reveal novel opportunities for NK cell–based immunotherapy.

Results

Loss of *Zhx2* leads to accumulation of mature NK cells in mice

We first detailed the *Zhx2* expression pattern in immune cells using a publicly available database. Notably, among members of the ZHX family, *ZHX2* was highly expressed in lymphocytes (Zhao et al., 2020; Fig. S1 A) and NK cells isolated from different tissues (Dogra et al., 2020; Fig. S1 B), indicating its role in NK cells.

To study the role of Zhx2 in NK cells, we crossed *Ncr1*-Cre mice (gift from Prof. Zhongjun Dong, Institute for Immunology, Tsinghua University, Beijing, China) with mice carrying floxed *Zhx2* alleles (gift from Prof. Brett T. Spear, Department of Microbiology, Immunology and Molecular Genetics, University of Kentucky, Lexington, KY) to generate an NK cell–specific knockout mouse referred to as the $Zhx2^{\Delta/\Delta}$ mouse. Western blot analysis confirmed the deletion of *Zhx2* in splenic NK cells (Fig. S1 C). Compared with WT ($Zhx2^{+/+}$) mice, a two- to threefold increase of $CD3^-NK1.1^+CD49b^+$ NK cells was observed in $Zhx2^{\Delta/\Delta}$ mice in the liver, spleen, and blood in terms of both relative ratios and absolute cell counts (Fig. 1, A and B). Similar results were seen when NK cells were gated as $CD3^-NK1.1^+$ cells (Fig. S1, D and E). We then examined the role of Zhx2 in NK cell maturation. As shown in Fig. 1, C–E, and Fig. S1, F and G, NK cell–specific *Zhx2* depletion led to an overall increase of the most mature $CD27^-CD11b^+$ NK cell population ($CD27^{low}$) in the liver, spleen, blood, and BM in both relative proportions and absolute cell numbers. The frequency of the $KLRG1^+$ mature NK subsets (pregated on $CD3^-NK1.1^+CD49b^+$ cells) was also significantly higher in the liver and spleen from $Zhx2^{\Delta/\Delta}$ mice than in those from $Zhx2^{+/+}$ mice (Fig. 1 F), suggesting a more mature phenotype of NK cells (Huntington et al., 2007a). To further verify the role of Zhx2 in NK cell maturation, an in vitro NK cell differentiation system was established with NK cells from tamoxifen-induced *Zhx2* knockout mice (*Cag-*$Zhx2^{\Delta/\Delta}$, obtained by crossing $Zhx2^{fl/fl}$ mice to the Cag^{cre} strain) and control *Cag-*$Zhx2^{+/+}$ mice (Fig. 1 G). Briefly, spleen NK cells were purified from *Cag-*$Zhx2^{+/+}$ and *Cag-*$Zhx2^{\Delta/\Delta}$ mice that received a 3-d i.p. injection of tamoxifen (T5648; Sigma-Aldrich) for in vitro culture for 5 d with 20 ng/ml IL-2 and 20 ng/ml IL-15. Western blot analysis confirmed the tamoxifen-induced deletion of *Zhx2* in splenic NK cells of *Cag-*$Zhx2^{\Delta/\Delta}$ mice (Fig. S1 H). Flow cytometry (FCM) results showed that, although the input NK cells from *Cag-*$Zhx2^{+/+}$ and *Cag-*$Zhx2^{\Delta/\Delta}$ mice at day 0 showed no difference in NK cell maturation (Fig. S1 I), *Zhx2* depletion in NK cells induced a greater proportion of the matured $CD27^{low}$ NK population after 5-d IL-15 stimulation (Fig. 1 H). Moreover, NK precursor (NKP) cells, which were characterized as $Lin^-CD244^+CD27^+CD122^+NK1.1^-$ (Tang et al., 2012), were unaltered in *Cag-*$Zhx2^{\Delta/\Delta}$ mice, excluding the role of Zhx2 in early steps of NK cell development (Fig. S1, J and K). Collectively, all these results suggest that Zhx2 restricts NK cell terminal maturation.

Zhx2 mediates a cell-intrinsic role in NK cell homeostasis

To explore whether Zhx2 is cell intrinsically required for NK cell maturation, mixed BM chimera experiments were performed (Fig. 2 A). Congenic BM cells ($CD45.2^+Zhx2^{\Delta/\Delta}$ and $CD45.1^+Zhx2^{+/+}$) were transferred into irradiated WT $CD45.1^+CD45.2^+$ recipients at a 1:1 ratio, and $CD3^-NK1.1^+CD49b^+$ NK cell chimerism was assessed in the spleen 8 wk after transfer. As displayed in Fig. 2 B, $CD45.2^+Zhx2^{\Delta/\Delta}$ BM cells reconstituted the NK cell compartment in the spleen better than those of $CD45.1^+Zhx2^{+/+}$ mice. Further FCM analysis showed that the increase of NK cells from $Zhx2^{\Delta/\Delta}$ BM cells was predominately in the $CD27^{low}$ NK population, which was coupled with a relative decrease of $Zhx2^{\Delta/\Delta}$-derived NK cells in double-positive (DP) stage (Fig. 2 C). Noncompetitive transplant, whereby $CD45.2^+Zhx2^{+/+}$ or $CD45.2^+Zhx2^{\Delta/\Delta}$ BM was transferred into $CD45.1^+$ WT congenic irradiated recipients (Fig. 2 D), demonstrated a similar increase in $CD45.2^+CD3^-NK1.1^+CD49b^+$ cells developing from the transferred $Zhx2^{\Delta/\Delta}$ BM after 8 wk (Fig. 2 E). The percentage of $CD27^{low}$ was also higher in the $Zhx2^{\Delta/\Delta}$ group (Fig. 2 F). Thus, we conclude that Zhx2 regulates NK cell homeostasis in a cell-intrinsic manner.

Enhanced effector functions of NK cells with *Zhx2* deficiency

NK cell maturation accompanies an enhancement of effector functions. Thus, we next assessed the functional effects of $Zhx2^{\Delta/\Delta}$ NK cells in vitro and in vivo. FCM analyses showed significantly reduced expression of inhibitory receptor NKG2A as well as the obviously increased expression of activating receptor NKG2D on splenic $Zhx2^{\Delta/\Delta}$ NK cells (Fig. 3 A). Upon

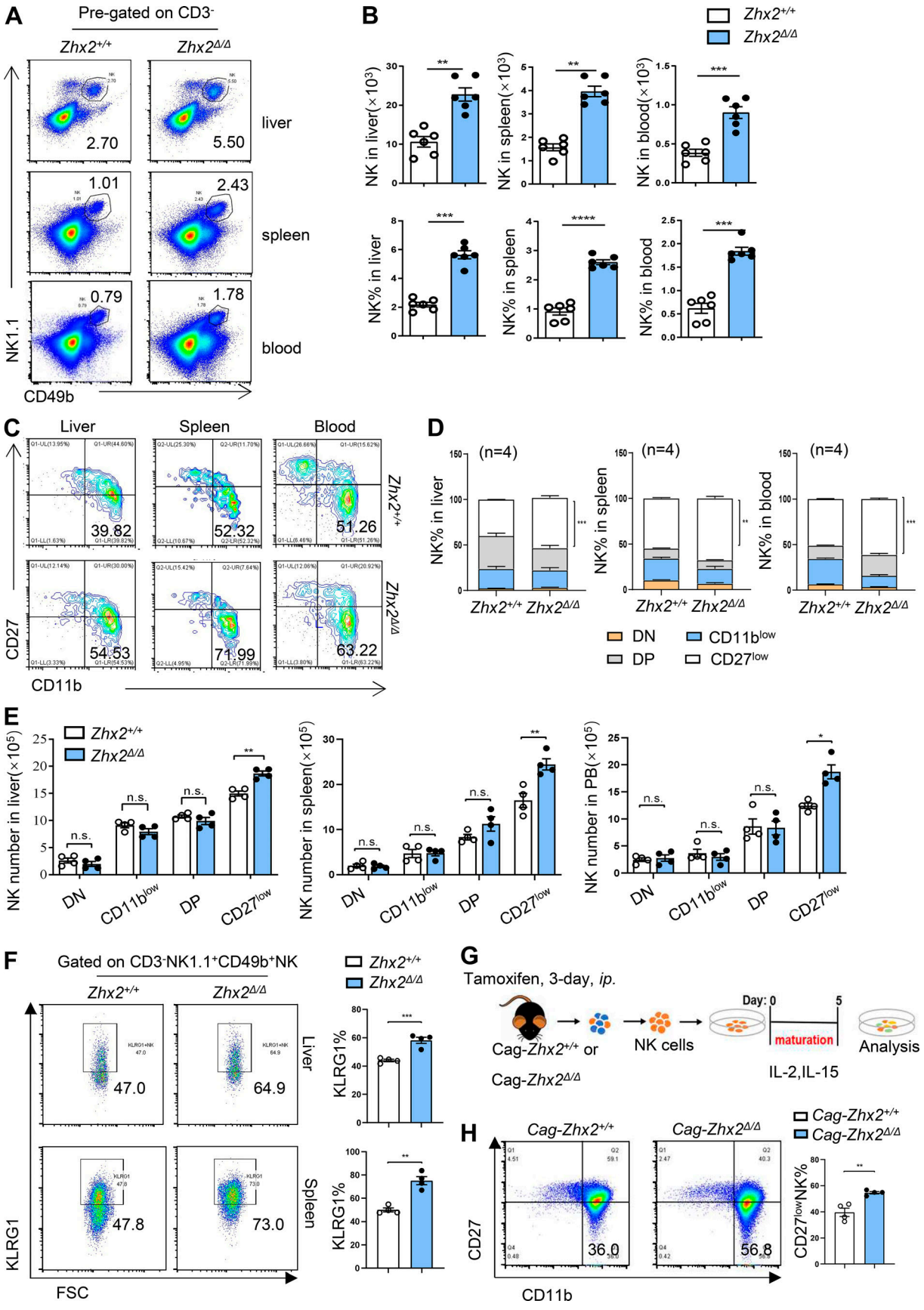

Figure 1. **Knockout of *Zhx2* in NK cells results in increased maturation of NK cells. (A and B)** FACS plots and bar graphs present percentages and absolute numbers of CD3⁻NK1.1⁺CD49b⁺ NK cells in the liver, spleen, and blood from *Zhx2*$^{+/+}$*Ncr1*-icre^{+} (*Zhx2*$^{+/+}$) and *Zhx2*$^{fl/fl}$*Ncr1*-icre^{+} (*Zhx2*$^{Δ/Δ}$) mice (representative of

at least three independent experiments). **(C–E)** FACS plots (C) and bar graphs of cell percentage (D) and cell number (E) depict NK cell subsets determined by expression of CD11b/CD27 in the liver, spleen, and blood from *Zhx2*$^{+/+}$ and *Zhx2*$^{\Delta/\Delta}$ mice (pregated on CD3$^-$NK1.1$^+$CD49b$^+$ NK subsets, representative of at least three independent experiments). DN, double negative. **(F)** Representative histograms showing KLRG1 expression in liver and spleen CD3$^-$NK1.1$^+$CD49b$^+$ NK cells from *Zhx2*$^{+/+}$ and *Zhx2*$^{\Delta/\Delta}$ mice. Graphs show the quantification of the percentage of KLRG1$^+$ NK cells (representative of three independent experiments). FSC, forward scatter. **(G)** Graphical representation of in vitro NK cell differentiation system using NK cells isolated from *Cag-Zhx2*$^{+/+}$ and *Cag-Zhx2*$^{\Delta/\Delta}$ mice. **(H)** Representative plots of expression of CD11b/CD27 in gated CD3$^-$NK1.1$^+$ cells and graph depicting percentages of CD27$^-$CD11b$^+$ cells (representative of two independent experiments). For all figures, dots represent individual mice or different cell replicates, and error bars represent SEM per group in one experiment. Data were analyzed using Student's *t* test (two-tailed paired *t* test). *, P < 0.05; **, P < 0.01; ***, P < 0.001; ****, P < 0.0001.

stimulation of anti-NK1.1, hepatic and splenic CD3$^-$NK1.1$^+$ NK cells from *Zhx2*$^{\Delta/\Delta}$ mice displayed markedly enhanced production of IFN-γ, TNF-α, CD107a, and granzyme than those from *Zhx2*$^{+/+}$ mice (Fig. 3 B). Real-time quantitative PCR (qPCR) with purified murine splenic NK cells verified the augmented production of effector molecules in *Zhx2*$^{\Delta/\Delta}$ NK cells (Fig. 3 C). The increased effector molecules were also detected in CD27^{low} NK cells from *Zhx2*$^{+/+}$ and *Zhx2*$^{\Delta/\Delta}$ mice (Fig. S2, A and B). Furthermore, splenic NK cells from control and *Zhx2*$^{\Delta/\Delta}$ mice were tested for their ability to kill mouse lymphoma Yac-1 cells. Supporting the notion that Zhx2 inhibits NK functions, NK cells from *Zhx2*$^{\Delta/\Delta}$ mice showed significantly higher killing activities against Yac-1 cells than NK cells from *Zhx2*$^{+/+}$ mice in both different effector/target (E:T) ratio and real-time cytotoxicity assays (Fig. 3, D and E). This was further validated with an in vivo killing experiment in which CFSE labeling Yac-1 cells were i.p. injected in either *Zhx2*$^{\Delta/\Delta}$ or *Zhx2*$^{+/+}$ mice. As shown in Fig. 3 F, there were fewer remaining Yac-1 cells in *Zhx2*$^{\Delta/\Delta}$ mice.

Next, we evaluated *Zhx2*$^{\Delta/\Delta}$ NK cell–mediated tumor elimination in vivo by s.c. injection of mouse hepatoma cell line Hepa1-6 cells into *Zhx2*$^{\Delta/\Delta}$ and *Zhx2*$^{+/+}$ mice, respectively. As shown in Fig. 3, G and H, larger tumors had evolved in *Zhx2*$^{+/+}$ mice, whereas a pronounced reduction of tumor mass was observed in *Zhx2*$^{\Delta/\Delta}$ mice.

To validate the role of ZHX2 in human NK cells, *ZHX2* overexpression and knockdown were performed in human NK cell line NK92 cells. As expected, overexpression of *ZHX2* decreased, whereas interference of *ZHX2* expression enhanced expression of functional molecules IFN-γ, TNF-α, granzyme, and perforin (Fig. S2, C and D). Also, ZHX2 inhibited the cytotoxicity of NK92 cells against target K562 cells (Fig. S2 E). Altogether, these data demonstrate that Zhx2 inhibits NK cell cytotoxicity and cytokine production.

Loss of *Zhx2* enhances NK cell viability

Our above data suggest that loss of *Zhx2* results in an increased number of terminal mature NK cells and subsequently augmented NK cell functions. We next investigated the mechanism of the increment of CD27^{low} NK cells in *Zhx2*$^{\Delta/\Delta}$ mice. To address that, splenic NK cells were purified from both *Zhx2*$^{+/+}$ and *Zhx2*$^{\Delta/\Delta}$ mice, and cell proliferation and survival were assessed. As shown in Fig. 4, A and C, both an ex vivo 5-ethynyl-2′-deoxyuridine (EdU) labeling assay and Ki67 staining did not detect any significant difference between NK cells from the two groups, indicating that Zhx2 does not influence NK cell proliferation. Also, all four stages of NK cells, including the mature CD27^{low} NK cells, showed no difference in EdU and Ki67 staining between *Zhx2*$^{+/+}$ and *Zhx2*$^{\Delta/\Delta}$ mice (Fig. 4, B and D). In contrast, an annexin V/7-AAD staining assay showed an obviously reduced number of apoptotic NK cells isolated from *Zhx2*$^{\Delta/\Delta}$ mice compared with those from control *Zhx2*$^{+/+}$ mice (Fig. 4 E). To confirm the apoptotic resistance of NK cells from *Zhx2*$^{\Delta/\Delta}$ mice, the apoptosis inducer cycloheximide (CHX) was added to NK cell culture. As shown in Fig. 4 F, upon CHX treatment, in vitro cultured *Zhx2*$^{\Delta/\Delta}$NK cells underwent less apoptosis than control cells at all detected time points. In accordance, RNA sequencing (RNA-seq) and gene set enrichment analysis (GSEA) using the Broad Hallmark gene set collection demonstrated significant enrichments for a gene set encoding apoptosis-related molecules in *Zhx2*$^{+/+}$ NK cells relative to their expression in the *Zhx2*$^{\Delta/\Delta}$ NK cell subset (Fig. 4 G).

We further asked whether Zhx2 contributes to the maintenance of NK cells in vivo. To this end, congenitally marked NK cells from *Zhx2*$^{+/+}$ or *Zhx2*$^{\Delta/\Delta}$ mice were labeled with CellTrace Violet (CTV) or CFSE, respectively, and then mixed in a 1:1 ratio and cotransferred into either C57BL/6 WT recipient mice (Fig. 4 H) or nonobese diabetic *Prkdc*^{em26}*IL2rg*^{em26}*/Gpt* (NSG; NOD-*Prkdc*^{em26}*IL2rg*^{em26}*/Gpt*) recipient mice (Fig. 4 I), which lack all lymphocytes but have abundant IL-15. FCM results showed a selective loss of *Zhx2*$^{+/+}$ NK cells in recipient mice. Concurrently, *Zhx2*$^{\Delta/\Delta}$ NK cells displayed increased viability compared with *Zhx2*$^{+/+}$ NK cells in the CD27^{low} subset (Fig. 4 J). These data underline the importance of Zhx2 in NK cell survival.

Zhx2 deficiency enhances NK cell response to IL-15 stimulation

IL-15 plays a crucial role in NK cell biology, including cell survival, maturation, and function (Marçais et al., 2014; Waldmann, 2015). We then examined whether Zhx2 participates in IL-15 signaling in NK cells. GSEA was performed comparing RNA-seq data of splenic NK cells purified from *Zhx2*$^{+/+}$ and *Zhx2*$^{\Delta/\Delta}$ mice to address gene expression related to IL-15 signaling. As shown in Fig. 5 A, *Zhx2*$^{\Delta/\Delta}$ NK cells demonstrated enrichment for genes associated with IL-15 signaling. IL-15 accesses its downstream signaling via a common γ subunit (CD132) and an IL-15Rβ chain (CD122; Mishra et al., 2014; Waldmann, 2015). FCM did not detect any difference in the expression of CD122 in NK cells with *Zhx2* deficiency (Fig. 5 B). We thus hypothesized that *Zhx2* deficiency might influence IL-15–initiated phosphorylation of STAT5 and the survival kinase AKT, two major signaling events stimulated by IL-15 (Marçais et al., 2014; Waldmann, 2015; Lin et al., 2017; Wang et al., 2019). Supporting this hypothesis, after in vitro stimulation of IL-15, NK cells isolated from *Zhx2*$^{\Delta/\Delta}$ mice displayed obvious increases in phosphorylated STAT5 and AKT compared with those from *Zhx2*$^{+/+}$ mice (Fig. 5 C). Furthermore, with the IL-15 treatment, *Zhx2*$^{\Delta/\Delta}$ NK cells showed significantly enhanced effector functions displaying as increased levels of

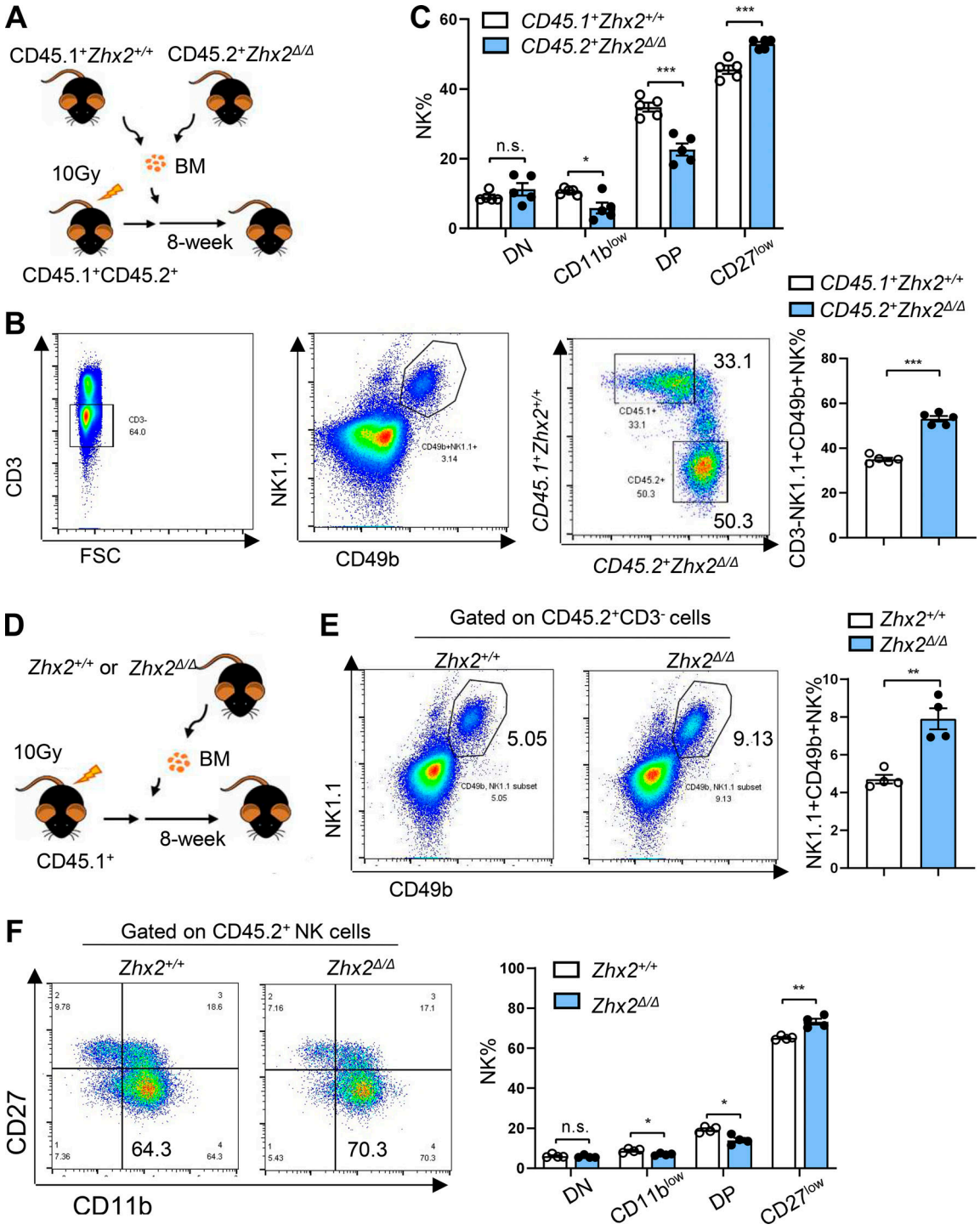

Figure 2. **Zhx2-mediated a cell-intrinsic role in NK cell homeostasis. (A)** Experimental design of congenic BM chimera assay. **(B and C)** FACS plots and bar graphs represent the ratio of CD45.2$^+$ and CD45.1$^+$ NK (pregated on CD3$^-$NK1.1$^+$CD49b$^+$ NK subsets; B) and the percentages of NK cell subsets (C) as retrieved from the spleen of mixed BM chimeras (representative of three independent experiments). FSC, forward scatter. **(D)** Representation of noncompetitive BM chimera. DN, double negative. **(E and F)** Representative flow plots and summary data showing the percentage of CD45.2$^+$CD3$^-$NK1.1$^+$CD49b$^+$ cells (E) and the percentages of NK cell subsets (F) as retrieved from the spleen of BM chimeras from *Zhx2*$^{+/+}$ and *Zhx2*$^{\Delta/\Delta}$ mice (representative of three independent experiments). For all figures, dots represent data from individual mice, and error bars represent SEM per group in one experiment. Data were analyzed using Student's *t* test (two-tailed paired *t* test). *, P < 0.05; **, P < 0.01; ***, P < 0.001.

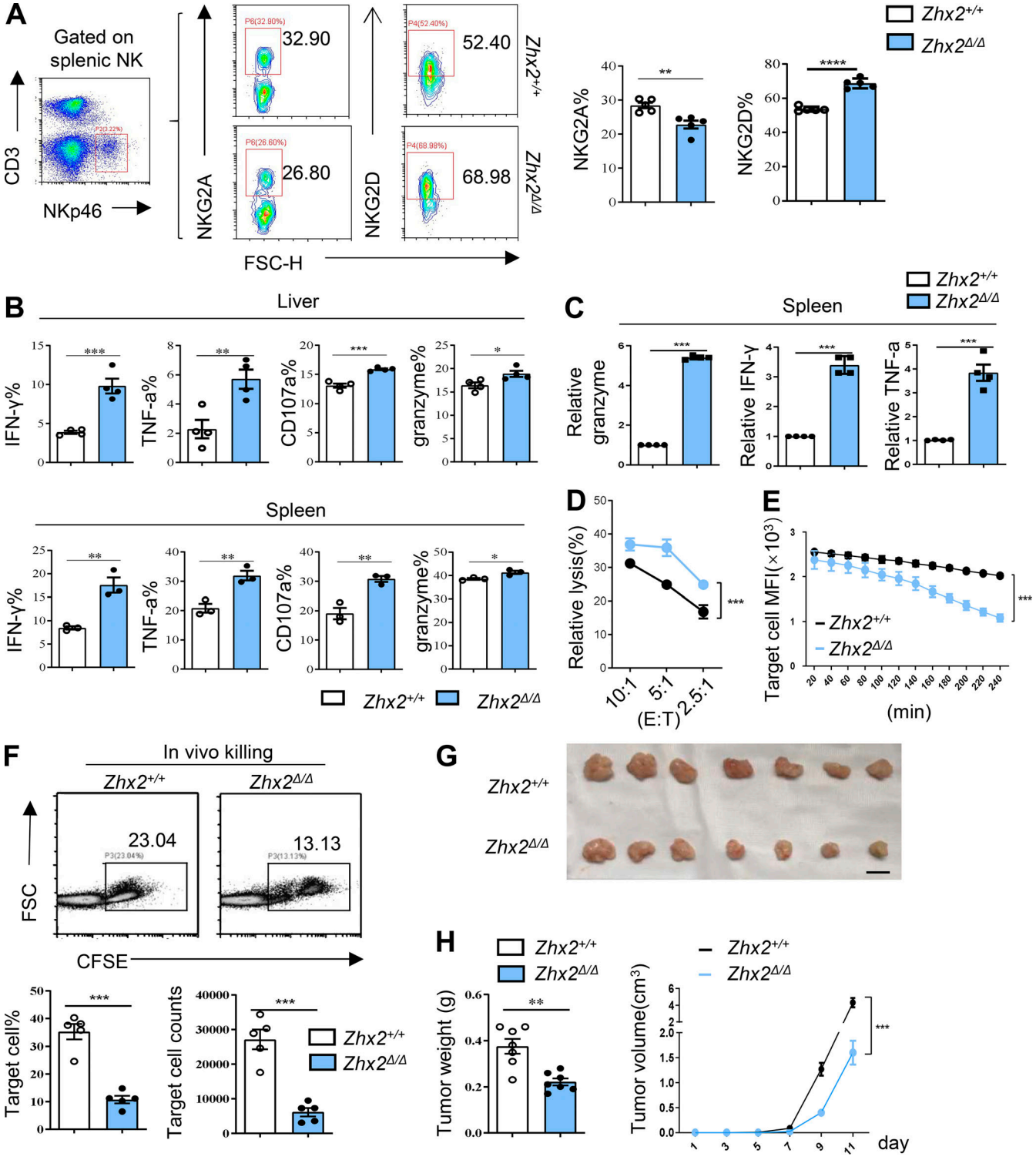

Figure 3. ***Zhx2* deficiency gives NK cells enhanced effector functions and promotes tumor immunosurveillance. (A)** Representative plots showing the expression of NKG2A and NKG2D in spleen NK cells from *Zhx2*$^{+/+}$ and *Zhx2*$^{\Delta/\Delta}$ mice. Graphs show the quantification of percentages of NKG2A^{+}/NKG2D^{+} NK cells (representative of three independent experiments). FSC-H, forward scatter height. **(B)** Percentages of indicated effector molecules accessed with FCM in anti-NK1.1–stimulated NK cells from the liver and spleen of *Zhx2*$^{+/+}$ or *Zhx2*$^{\Delta/\Delta}$ mice (representative of three independent experiments). **(C)** Real-time qPCR analysis of expression of *granzyme*, *IFN-γ*, and *TNF-α* in splenic NK cells from *Zhx2*$^{+/+}$ or *Zhx2*$^{\Delta/\Delta}$ mice (representative of two independent experiments). **(D and E)** FACS analysis of the cytotoxicity of the indicated NK cells against CFSE-labeled Yac-1 cells. D shows the relative lysis of Yac-1 cells detected by 7-AAD staining at different E:T ratios (representative of three independent experiments). E shows real-time cytotoxicity assays against CFSE-labeled Yac-1 cells at 5:1 E:T ratio. Yac-1 cell growth was measured with the Real-Time Cell Analyzer multiple plate system (PerkinElmer; representative of three independent experiments). MFI, mean fluorescence intensity. **(F)** In vivo killing assays were performed by i.p. injection of CFSE-labeled Yac-1 cells in the indicated mice. Representative plots and frequencies and numbers of remaining CFSE-labeled Yac-1 cells in the peritoneal cavity are displayed (representative of two independent experiments).

(G and H) Xenograft assays in *Zhx2*$^{+/+}$ and *Zhx2*$^{\Delta/\Delta}$ mice (representative of two independent experiments). G shows ex vivo tumor imaging. Scale bar: 1 cm. H depicts the tumor weight and growth of s.c. inoculated Hepa1-6 cells in the indicated mice. Each dot represents data from an individual mouse, and error bars represent SEM per group in one experiment. Data were analyzed using Student's *t* test (two-tailed paired *t* test) for A–C, F, and H (left), and using two-way ANOVA for D, E, and H (right). *, P < 0.05; **, P < 0.01; ***, P < 0.001

CD107a and IFN-γ. The augmented responses of *Zhx2*$^{\Delta/\Delta}$ NK cells were particularly evident when IL-15 was present at a high concentration (50 ng/ml; Fig. 5 D). Consistent with the notion that IL-15 boosts bioenergetic metabolism and promotes the survival of NK cells (Kobayashi and Mattarollo, 2019), the Seahorse XF Analyzer detected higher maximum respiration in IL-15–stimulated *Zhx2*$^{\Delta/\Delta}$ NK cells (Fig. 5 E), whereas FCM showed a decrease of apoptosis in IL-15–stimulated NK cells from *Zhx2*$^{\Delta/\Delta}$ mice compared with those from *Zhx2*$^{+/+}$ mice (Fig. 5 F).

To further verify the depressing function of Zhx2 in the IL-15 pathway, the selective IL-15 signaling STAT5 inhibitor (STAT5-Inh, HY-102048; MedChemExpress) was employed. As previously reported (Juen et al., 2017), STAT5-Inh inhibited the phosphorylation of STAT5 (Fig. S3 A) and enhanced apoptosis in NK cells (Fig. 5 G). More important, treatment with STAT5-Inh not only largely rescued the IL-15–triggered up-regulation of the phosphate STAT5 level in *Zhx2*$^{\Delta/\Delta}$ NK cells (Fig. S3 A) but also eliminated the difference of IL-15–induced cell apoptosis between *Zhx2*$^{+/+}$ and *Zhx2*$^{\Delta/\Delta}$ NK cells (Fig. 5 G). Accordingly, STAT5-Inh almost completely destroyed the enhanced production of CD107a and IFN-γ expression in *Zhx2*$^{\Delta/\Delta}$ NK cells (Fig. S3 B). Taken together, phenotypic, functional, and metabolic analyses concordantly demonstrate that Zhx2 restrains the NK cell response to IL-15.

Zhx2 directly inhibits *Zeb2* transcription during NK cell development

Zhx2 has been demonstrated as a TF (Yue et al., 2012). To further identify the direct target of Zhx2 and elucidate the underlying mechanism by which Zhx2 regulates NK cells, RNA-seq and assay for transposase-accessible chromatin using sequencing (ATAC-seq) were performed using *Zhx2*$^{+/+}$ and *Zhx2*$^{\Delta/\Delta}$ splenic NK cells. The volcano plot derived from RNA-seq showed that 1,642 genes were significantly altered in *Zhx2*$^{\Delta/\Delta}$ NK cells compared with *Zhx2*$^{+/+}$ NK cells (1,325 up-regulated and 317 down-regulated; P ≤ 0.05; Fig. 6 A). To obtain more in-depth insight into the impact of *Zhx2* loss on NK cell development, we used GSEA comparing transcriptional profiles of *Zhx2*$^{+/+}$ NK cells and *Zhx2*$^{\Delta/\Delta}$ NK cells against previously defined signature genes of DP or CD27^{low} NK cells (Meinhardt et al., 2015). Fig. 6 B shows that the set of *Zhx2*$^{\Delta/\Delta}$ NK cells was preferentially active in the CD27^{low}subset, whereas the set of *Zhx2*$^{+/+}$ NK cells was preferentially active for the immature DP subset, supporting the role of Zhx2 in restricting NK cell maturation.

A total of 6,426 peak genes were differentially detected in ATAC-seq of *Zhx2*$^{\Delta/\Delta}$ NK cells compared with *Zhx2*$^{+/+}$ NK cells. We centered all the differential ATAC peaks according to the transcription start sites (TSSs) of the closest genes, and the resulting heatmap of the average ATAC-seq signals shows an increased openness in the *Zhx2*$^{\Delta/\Delta}$ strains around the TSS with a peak just upstream of the TSS (Fig. S4 A). In gene ontology (GO) analyses, immune response and inflammatory response were significantly overrepresented, further supporting the involvement of Zhx2 in NK cell responses (Fig. S4 B). These data indicated that the lack of *Zhx2* prompted an altered transcriptional network to become operational in NK cells.

To identify the direct target of Zhx2, we performed a cluster analysis of sharing genes in ATAC-seq and RNA-seq data from *Zhx2*$^{+/+}$ and *Zhx2*$^{\Delta/\Delta}$ splenic NK cells, as well as reported CD27^{low}/DP NK represented genes (Meinhardt et al., 2015). As shown in Fig. 6 C, most genes were specific to only one or two clusters. However, nine genes changed in all three clusters, which are believed to be Zhx2-regulated genes in NK cell maturation. The Zhx2-mediated regulation of these nine genes was further verified with real-time qPCR with purified splenic CD3$^-$NK1.1$^+$ NK cells from *Zhx2*$^{\Delta/\Delta}$ and *Zhx2*$^{+/+}$ mice (Fig. S4 C). We then compared the expression levels of these nine genes during NK cell development using reported data (Meinhardt et al., 2015). Very interestingly, consistent with the role of Zhx2 in limiting NK cell maturation, two (*Tcf7*, *Slamf6*) of three genes, which were decreased in *Zhx2*-deficient cells, were gradually decreasing during NK cell development, whereas Zhx2 down-regulated genes, including *Itgam*, the encoding gene of well-known maturation marker CD11b, as well as *Emilin2*, *Fbxl2*, and *Zeb2*, showed their highest expression in the matured CD27^{low} NK cells (Fig. S4 D). Notably, among six of the Zhx2 down-regulated targets, *Zeb2* was the most suppressed TF (Fig. S4 C).

Researchers in a previous study reported that Zeb2 is indispensable for the survival of mature NK cells and essential for CD27^{low} NK cell maturation (van Helden et al., 2015), which coincides with the role of Zhx2 in NK cells. To verify *Zeb2* as the direct target of Zhx2, several molecular biology methods were employed. Real-time qPCR showed the negative correlation of *Zeb2* and *Zhx2* mRNA expression in NK cells isolated from *Zhx2*$^{\Delta/\Delta}$ mice and *Zhx2*$^{+/+}$ mice (Fig. 6 D). In accordance with this, cotransfection and a dual luciferase assay demonstrated that *ZHX2* overexpression markedly inhibited *ZEB2* promoter activity in NK92 cells (Fig. 6 E). Furthermore, a chromatin immunoprecipitation (ChIP) assay performed with anti-ZHX2 and NK92 cell lysate demonstrated that ZHX2 significantly occupied with *ZEB2* promoter in NK92 cells (Fig. 6 F). The Zhx2-mediated transcription inhibition of *Zeb2* was further confirmed with GSEA comparing our RNA-seq data and reported data (Dominguez et al., 2015). As shown in Fig. 6 G, *Zeb2*–up-regulated transcripts were greatly enriched in *Zhx2*$^{\Delta/\Delta}$ subsets (Fig. 6 G). Consistently, ATAC-seq data showed a higher accessibility of the *Zeb2* promoter region in *Zhx2*$^{\Delta/\Delta}$ NK cells than that in *Zhx2*$^{+/+}$ NK cells (Fig. 6 H). All these results suggested that Zhx2 is capable of binding to the *Zeb2* locus, thus regulating *Zeb2* transcription.

To validate the involvement of Zeb2 in Zhx2-mediated regulation of NK cell maturation and function, *Zeb2* interference was performed by using a lentivirus in splenic NK cells from

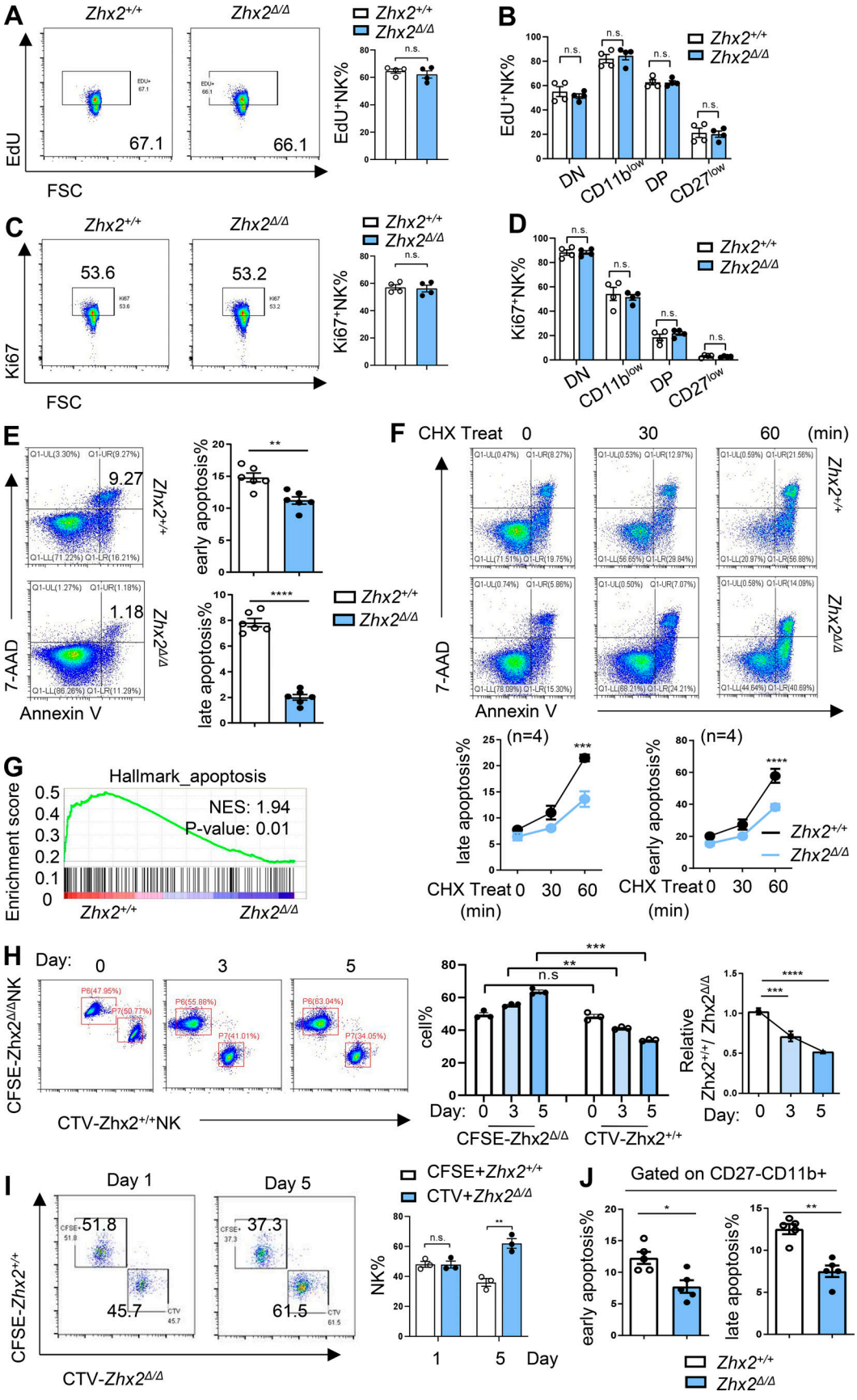

Figure 4. **Loss of *Zhx2* promotes NK cell survival. (A–D)** FCM analysis of EdU (A and B) and Ki67 (C and D) levels in $Zhx2^{+/+}$ and $Zhx2^{\Delta/\Delta}$ splenic NK cells cultured for 12 h with 5 ng/ml IL-15 (representative of three independent experiments). A and C are representative FACS plots (left) and summary data (right)

showing the percentage of EdU$^+$ NK cells (A) and Ki67$^+$NK cells (C). B and D show EdU$^+$ level (B) and Ki67$^+$ level (D) in NK subsets determined by CD11b/CD27 of the *Zhx2*$^{+/+}$ and *Zhx2*$^{\Delta/\Delta}$ groups. DN, double negative; FSC, forward scatter. **(E and F)** FACS plots and graphs show NK cell viability determined by annexin V/7-AAD staining (representative of at least two independent experiments; n = 4 in F). Splenic NK cells from *Zhx2*$^{+/+}$ and *Zhx2*$^{\Delta/\Delta}$ mice were either ex vivo assayed (E) or pretreated with CHX for the indicated times (F). **(G)** GSEA of *Zhx2*$^{+/+}$ and *Zhx2*$^{\Delta/\Delta}$ NK cell bulk RNA-seq data. The normalized enrichment score (NES) and FDR are shown. **(H and I)** NK cells isolated from *Zhx2*$^{+/+}$ and *Zhx2*$^{\Delta/\Delta}$ mice were labeled with CTV or CFSE and adoptively transferred into C57BL/6 hosts (H) or NSG hosts (I). FACS plots and graphs illustrate the percentages and the ratios of *Zhx2*$^{+/+}$ and *Zhx2*$^{\Delta/\Delta}$ NK cells at the indicated time points, with day 0 as the time of adoptive transfer (representative of at least two independent experiments). **(J)** FACS plots show annexin V/7-AAD staining on CD27$^-$CD11b$^+$ NK subsets. Graphs depict percentages of early and late apoptosis (representative of three independent experiments). Dots represent data from individual mice, and error bars represent SEM per group in one experiment. Data were analyzed using Student's t test (two-tailed paired t test). *, P < 0.05; **, P < 0.01; ***, P < 0.001; ****, P < 0.0001.

Zhx2$^{+/+}$ and *Zhx2*$^{\Delta/\Delta}$ mice, and the splenic NK cells were then transferred to irradiated host C57BL/6 WT mice. As shown in Fig. 6, I and J, *Zeb2* knockdown significantly dampened the enrichment of the CD27^{low} NK subset and augmented CD107a expression in the *Zhx2*$^{\Delta/\Delta}$ group. The interference efficiency of *Zeb2* was detected by Western blot analysis (Fig. S4 E). All these data illustrate that Zhx2 inhibits NK cell maturation and function by binding to the *Zeb2* promoter, thus leading transcriptional repression of *Zeb2*.

Better control of tumor growth by NK cells with *Zhx2* deletion

It has been well established in previous studies that blockade of NK cell maturation impairs NK cells' antitumor potential (Platonova et al., 2011; Richards et al., 2006). We wondered whether ZHX2 participates in this process. To address this, we analyzed The Cancer Genome Atlas (TCGA) hepatocellular carcinoma (HCC) dataset for NK cell abundance using specific gene sets, including *GZMH*, *GZMB*, *KLRD1*, *PRF1*, *NCR1*, *NMUR1*, *GNLY*, *CD160*, and *TBX21*, for identifying NK cells (https://xcell.ucsf.edu/; Aran et al., 2017). As shown in Fig. 7 A, high *ZHX2* expression in NK subsets correlated with a low frequency of TINK cells, and, vice versa, tumors with more TINK cells displayed less *ZHX2* expression. Furthermore, patients with low *ZHX2* expression showed better survival than those with high *ZHX2* in NK cells (Fig. 7 B).

To define whether Zhx2 participates in the regulation of TINK cells, a murine model of orthotopically HCC was created, and NK cells were harvested for FCM (Fig. S5 A). As shown in Fig. S5 B, the percentage of CD3$^-$NK1.1$^+$ TINK cells from *Zhx2*$^{\Delta/\Delta}$ mice was significantly higher than that in the *Zhx2*$^{+/+}$ group. Moreover, terminally mature NK cell subsets (CD27^{low}) displayed an increase in tumors of *Zhx2*$^{\Delta/\Delta}$ mice (Fig. S5 C). Also, TINK cells from the *Zhx2*$^{\Delta/\Delta}$ mice had a marked increase in expression of the effector molecule CD107a (Fig. S5 D). These findings demonstrated that Zhx2 negatively regulates the function and maturation of NK cells in the tumor microenvironment, which is strictly related to tumor immune evasion.

We then sought to determine whether the deletion of *Zhx2* would generate more functional and long-survival NK cells to protect against cancer. To address that, both an s.c. hepatoma homograft and a lung metastasis model were performed to assess the antitumor capacity of *Zhx2*$^{\Delta/\Delta}$ NK cells. As shown in Fig. 7, C–E, transfer of splenic NK cells from *Zhx2*$^{\Delta/\Delta}$ mice greatly suppressed the growth of Hepa1-6 s.c. homograft. Also, *Zhx2*-deficient NK cells significantly reduced lung metastasis of B16-F10 melanoma (Fig. 7, F–H). The number of metastatic nodules in the lung was significantly reduced in mice that received transfer of *Zhx2*$^{\Delta/\Delta}$ splenic NK cells (Fig. 7, F and G), and the overall survival of the mice treated with *Zhx2*$^{\Delta/\Delta}$ NK cells was also significantly longer (Fig. 7 H).

To verify whether *ZHX2* could be a potential intervention target with the aim of enhancing NK cell immunosurveillance in tumor therapy, two human HCC models were set up in NSG mice. First, HepG2-luciferase cells (5 × 10^6) were i.p. injected, and, in the meantime, 2 × 10^6 NK92 cells infected with lentiviral vector expressing negative control shRNA (LV-shNC) or lentiviral vector expressing shRNA agaist *ZHX2* (LV-sh*ZHX2*) were transferred (Fig. 7 I). The results of a D-luciferin–based bioluminescence assay showed that transfer of NK92 cells infected with LV-sh*ZHX2* greatly suppressed the growth of peritoneal hepatoma xenografts across time (Fig. 7 J). The overall survival of the LV-sh*ZHX2* group was also significantly longer (Fig. 7 K). Similar results were obtained with an s.c. HCC xenograft model. Briefly, human HCC cell line Huh7 cells (5 × 10^6) were s.c. injected into the axilla of NSG mice, and, 1 wk afterward, 2 × 10^6 indicated NK92 cells were transfused via the caudal vein (Fig. 7 L). As shown in Fig. 7, L and M, significantly smaller tumors were found in the mice that received LV-sh*ZHX2* NK92 cell treatment. These findings highlight the therapeutic potential of antitumor immunity of *ZHX2*-deficient NK cells. ZHX2 may be a new target based on the adoptive transfer of NK cells.

Discussion

NK cells are innate immune cells with immunosurveillance and immunoregulatory functions. The development and maturation of NK cells are harmoniously controlled by a complex transcriptional regulatory network (Brillantes and Beaulieu, 2019). In the present study, we identified Zhx2 as a novel negative regulator of NK cell maturation. In the absence of *Zhx2*, NK cells are driven toward terminal differentiation and are resistant to apoptosis. Mechanically, Zhx2 controls IL-15 signaling and transcription of *Zeb2*, a TF identified as a major driver of CD27^{low} NK cell differentiation (Dominguez et al., 2015). Our data add a novel mechanism to TF-mediated NK cell maturation.

Zhx2 is an understudied protein that has been ascribed to have a transcriptional function on the basis of tumor suppressor (Liu et al., 2015; Yue et al., 2012). Literature has shown Zhx2 functions in the immune system, including macrophage regulation and B cell development (Hystad et al., 2007; Nagel et al., 2015; Nagel et al., 2014; Wang et al., 2020; Wu et al., 2020a). Our results highlight the role of Zhx2 in the restriction of NK cell

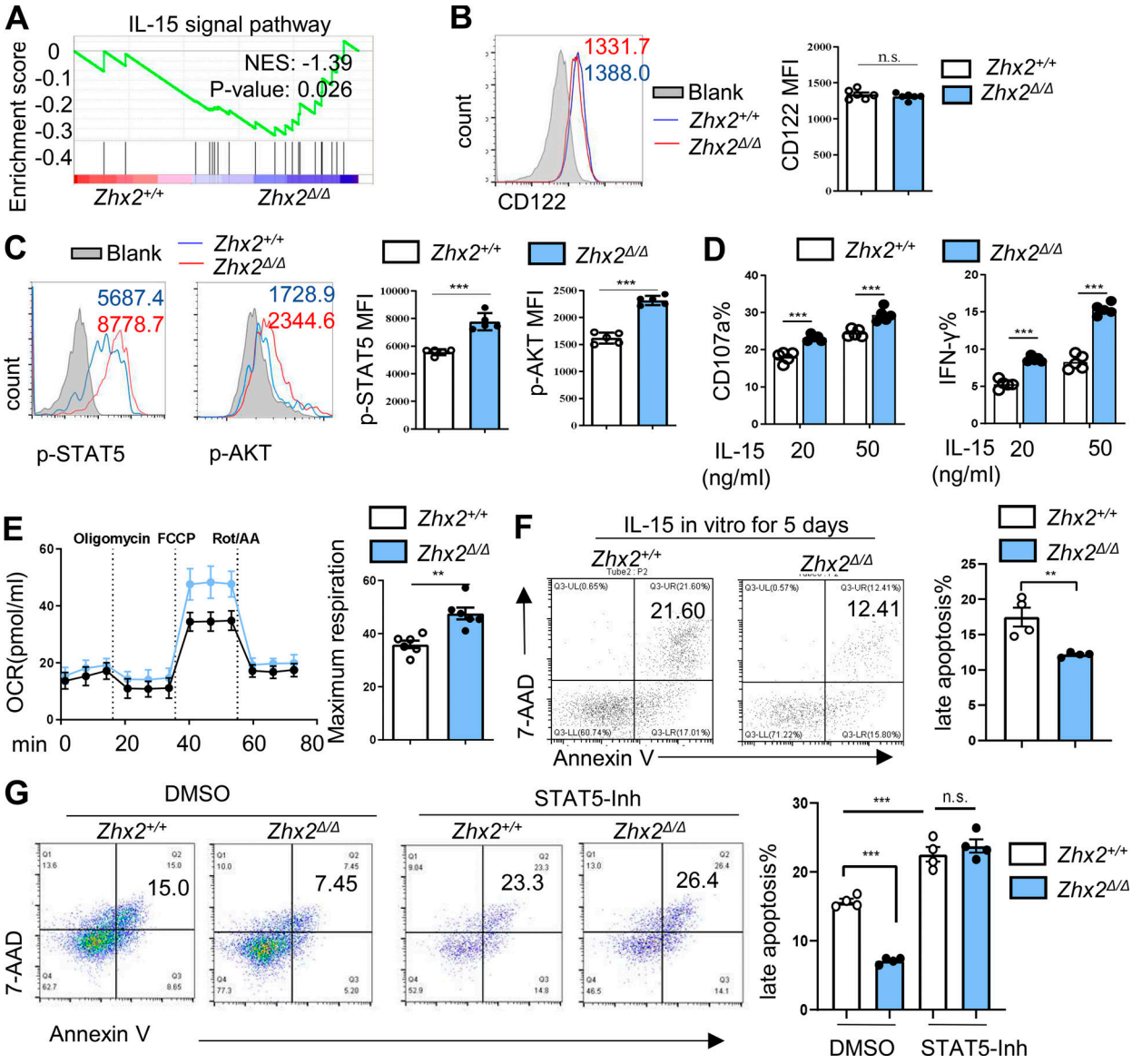

Figure 5. ***Zhx2* loss enhances NK response to IL-15 stimulation. (A)** GSEA of *Zhx2* mRNA expression and IL-15 signaling–related gene signatures. NES, normalized enrichment score. **(B)** FACS plots and graph show CD122 expression levels in gated CD3⁻NK1.1⁺ cells (representative of three independent experiments). MFI, mean fluorescence intensity. **(C)** FACS plots and graphs depict STAT5 (Tyr694) and AKT (Tyr308) phosphorylation in gated CD3⁻NK1.1⁺ cells after in vitro stimulation with IL-15 (representative of three independent experiments). **(D)** FCM analysis for CD107a and IFN-γ expression in splenic NK cells stimulated with the indicated concentrations of IL-15 (representative of two independent experiments). **(E)** Oxygen consumption rate (OCR) and maximum respiration of purified *Zhx2*$^{+/+}$ and *Zhx2*$^{Δ/Δ}$ NK cells activated in vitro with IL-15 (representative of two independent experiments). Data shown were obtained under basal conditions and in response to the indicated molecules. FCCP, carbonyl cyanide 4-(trifluoromethoxy)phenylhydrazone. **(F and G)** Representative FACS plots and graph show the percentage of apoptotic cells (annexin V⁺7-AAD⁺) among *Zhx2*$^{+/+}$ and *Zhx2*$^{Δ/Δ}$ NK cells. F shows that NK cells were cultured for 5 d with the presence of 5 ng/ml IL-15 (representative of two independent experiments). G shows that NK cells were stimulated with IL-15 in the presence of DMSO or STAT5-Inh (10 mM). FCM analysis of NK cell viability is shown (representative of two independent experiments). Dots represent data from individual mice, and error bars represent SEM per group in one experiment. Data were analyzed using Student's *t* test (two-tailed paired *t* test). **, P < 0.01; ***, P < 0.001.

maturation. We found that Zhx2 was abundantly expressed in NK cells. With the absence of Zhx2, NK cells exhibited an intrinsic enhanced maturation mainly affecting the number of the most mature subsets. Concurrently, *Zhx2* loss promoted the NK cell receptor repertoire and enhanced NK cell cytotoxicity and cytokine production. Although Zhx2 has been well recognized as a TF controlling cell proliferation–related genes in tumor cells (Shen et al., 2008; Yue et al., 2012), our ex vivo results and RNA-seq data showed that Zhx2 did not affect NK cell proliferation. Notably, our results showed that *Zhx2* knockout promotes NK cell sensitivity to IL-15, the crucial cytokine maintaining NK cell proliferation (Marçais et al., 2014); however, we did not find differences in IL-15–stimulated proliferation of *Zhx2*$^{+/+}$ and *Zhx2*$^{Δ/Δ}$ NK cells. In fact, *Zhx2*-decifient NK cells displayed reduced apoptosis both in vivo and in vitro in the presence of IL-15 stimulation, leading to prolonged survival. This is consistent

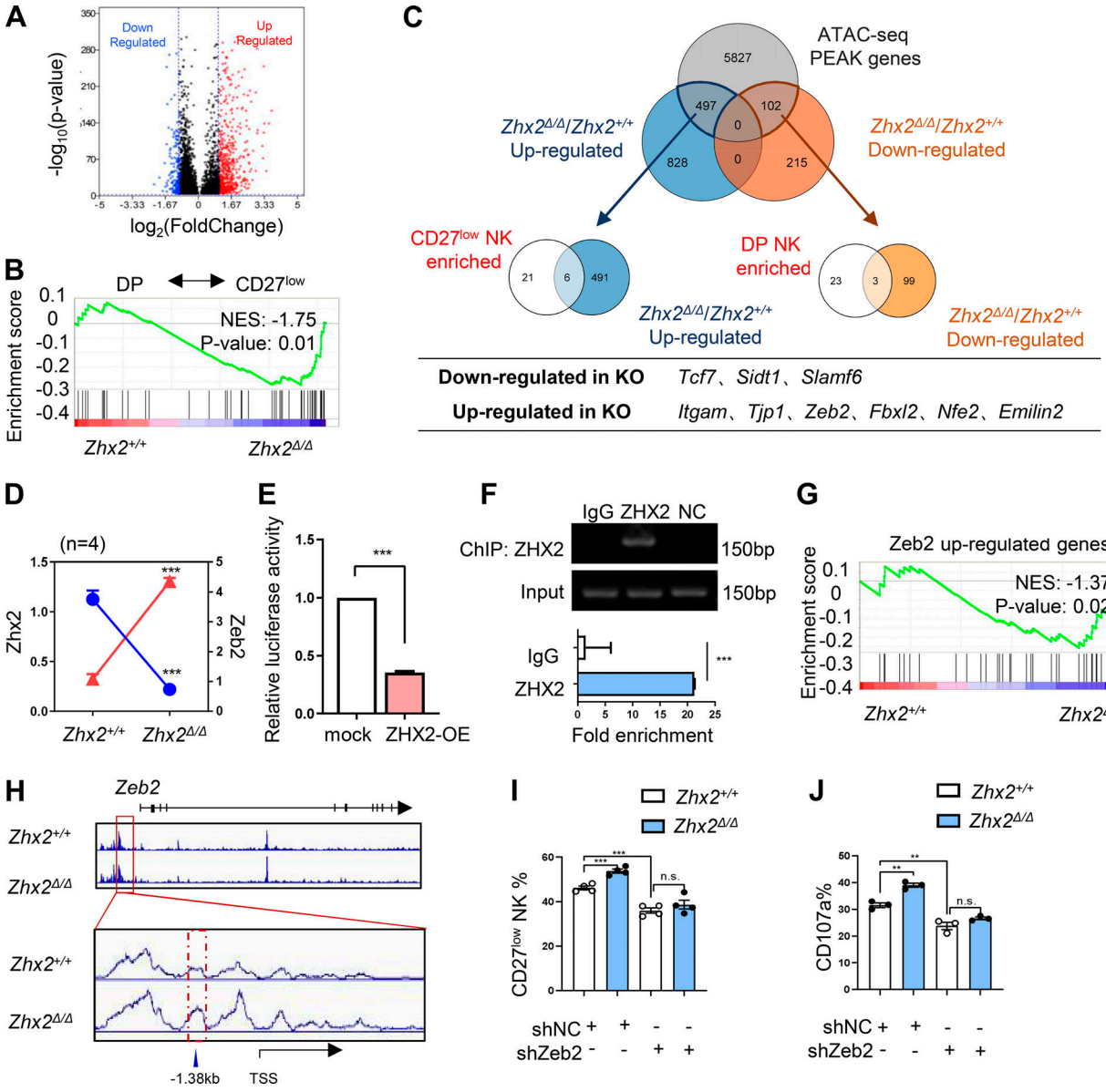

Figure 6. **Zhx2 directly represses *Zeb2* transcription during NK cell development. (A and B)** RNA-seq with purified splenic NK cells from $Zhx2^{+/+}$ and $Zhx2^{\Delta/\Delta}$ mice. A shows a volcano plot (log_2 [fold change] versus $-log_{10}$ [P value]). Fold change determinant is Log_2MEANFPKM ($Zhx2^{\Delta/\Delta}/Zhx2^{+/+}$). B shows the results of GSEA of DP NK ($CD27^+CD11b^+$) or $CD27^{low}$ NK ($CD27^-CD11b^+$) represented genes. RNA-seq data of DP and $CD27^{low}$ NK are adopted from Gene Expression Omnibus accession no. GSE45842. NES, normalized enrichment score. **(C)** Venn diagram showing shared genes in RNA-seq and ATAC-seq of $Zhx2^{+/+}$/ $Zhx2^{\Delta/\Delta}$ NK cells and reported NK cell maturation–related genes (Gene Expression Omnibus accession no. GSE45842). A subset of genes for different profiles is highlighted. **(D)** Real-time RT-qPCR showing *Zeb2* expression level in $Zhx2^{+/+}$ and $Zhx2^{\Delta/\Delta}$ NK cells (representative of three independent experiments). **(E)** Luciferase reporter gene assays were performed in HEK293T cells cotransfected with *ZHX2*-encoding (*ZHX2*-OE [overexpression]) or empty (mock) vector and *ZEB2* promoter reporter plasmid containing −2,000 to −100 nt of *Zeb2* gene (n = 6, representative of three independent experiments). **(F)** ChIP assay of ZHX2 binding to the *ZEB2* promoter in human NK92 cells. PCR primers were designed across the region around −1,438 to −1,276 nt shown in H as a red dashed line to amplify the ZHX2-binding region. Primers in the β-actin exon region were used as a negative control (NC). qPCR analyzed the quantities of fold change (representative of at least three independent experiments). **(G)** GSEA of *Zhx2* mRNA expression in RNA-seq data from $Zhx2^{+/+}$ and $Zhx2^{\Delta/\Delta}$ NK cells and reported *Zeb2*-repressed gene signatures (Gene Expression Omnibus accession no. GSE72162). **(H)** Integrative Genomics Viewer (IGV) screenshot showing *Zeb2* locus in $Zhx2^{+/+}$ and $Zhx2^{\Delta/\Delta}$ NK cells (from ATAC-seq with $Zhx2^{+/+}$ and $Zhx2^{\Delta/\Delta}$ NK cells). TSS, one open peak in $Zhx2^{\Delta/\Delta}$ NK cells, and the primer region for ChIP-qPCR (red dashed line) are shown. **(I and J)** Adoptive transfer assay. Splenic NK cells (5×10^6) from $Zhx2^{+/+}$ or $Zhx2^{\Delta/\Delta}$ mice pretreated with mock lentivirus (shNC)/ *Zeb2* interference lentivirus (sh*Zeb2*) were transferred into C57BL/6 recipients. Graph shows the percentage of recipient splenic $CD27^-CD11b^+$ ($CD27^{low}$) NK cells (I) and CD107a expression (J; representative of two independent experiments). Dots represent data from individual mice, and error bars represent SEM per group in one experiment. Data were analyzed using Student's t test (two-tailed paired t test). **, P < 0.01; ***, P < 0.001.

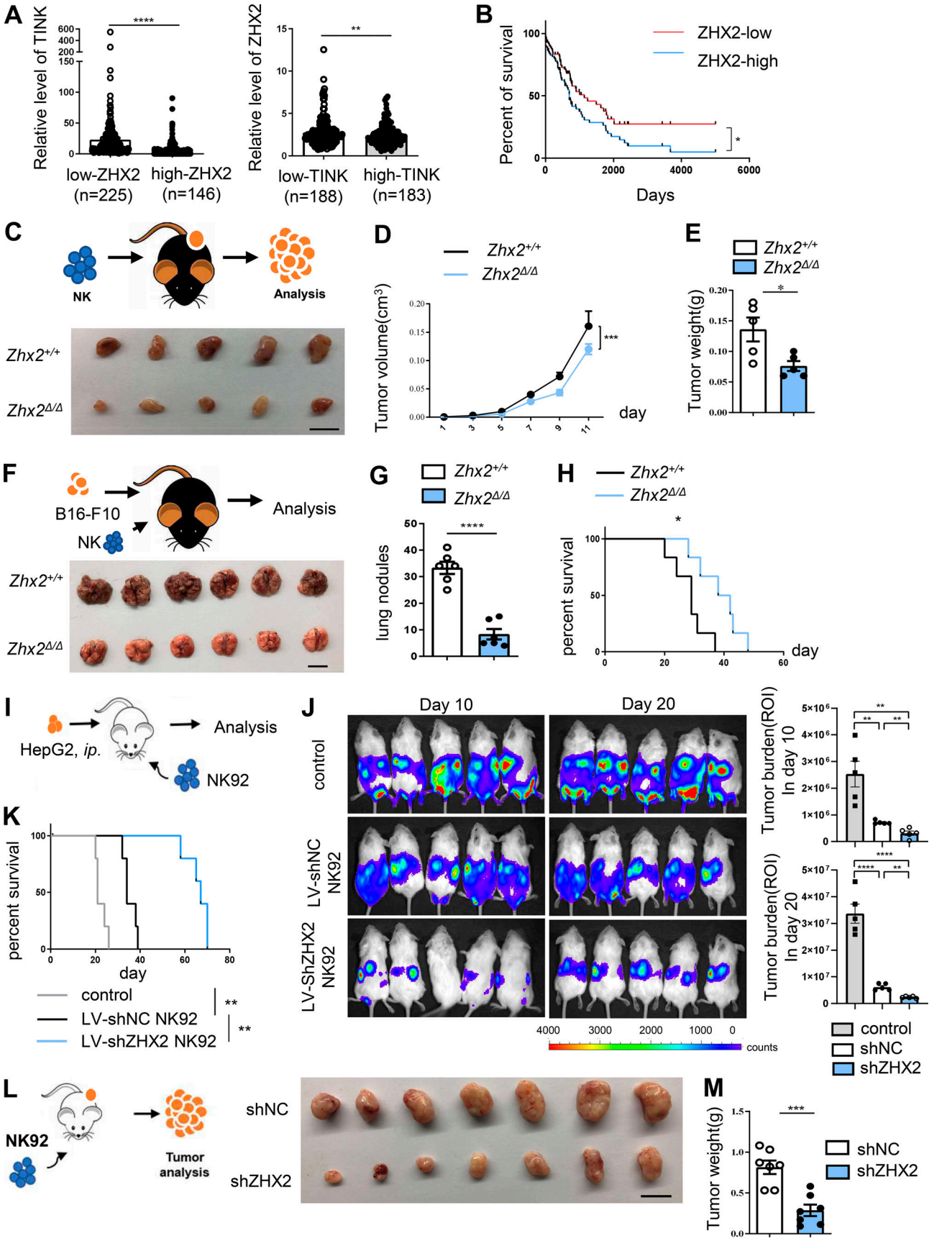

Figure 7. ***Zhx2* deletion boosts NK cell antitumor immunity. (A and B)** Analysis of 371 biologically independent HCC samples from a TCGA dataset. A shows the results of analysis of *ZHX2* expression related to intratumoral NK cell level in HCC patients. B shows the results of Kaplan-Meier analysis of overall survival

in patients in the discovery cohort classified by *ZHX2* expression. **(C–E)** Tumor growth and weight in C57BL/6 mice s.c. transplanted with Hepa1-6 cells, which were injected via the tail vein with purified NK cells from $Zhx2^{+/+}$ or $Zhx2^{\Delta/\Delta}$ mice (representative of two independent experiments). Experimental design, in vitro tumor image (C), tumor growth (D), and weight (E) are shown. Scale bar: 1 cm. **(F–H)** B16-F10 cells (2×10^5) were tail vein injected into C57BL/6 mice. 3 d later, mice were treated with 1×10^6 $Zhx2^{+/+}$ or $Zhx2^{\Delta/\Delta}$ NK cells with tail vein injection (representative of two independent experiments). The experimental design and in vitro tumor imaging (F), lung nodules (G), and survival curves (H) are shown. Scale bar: 1 cm. **(I–K)** Human HCC mouse models were established by i.p. injection of human HepG2-luciferase cells (5×10^6) and transfer of 2×10^6 LV-shNC- or LV-sh*ZHX2*-NK92 cells. Experimental design (I), tumor burden at day 10 and day 20 (J), and survival curves (K) are shown. ROI, region of interest. **(L and M)** Human HCC mouse models were established by s.c. injection of human Huh7 cells (5×10^6) and transfer of 2×10^6 LV-shNC- or LV-sh*ZHX2*-NK92 cells. Experimental design, tumor image (L), and weight (M) are shown. Scale bar: 1 cm. Dots represent data from individual mice; error bars, SEM per group in one experiment. Data were analyzed using Student's *t* test (two-tailed paired *t* test) in A, E, G, J, and M; using log-rank (Mantel-Cox) test in B, H, and K; and using two-way ANOVA in D. *, $P < 0.05$; **, $P < 0.01$; ***, $P < 0.001$; ****, $P < 0.0001$.

with a previous report showing increased apoptosis in *Zhx2*-null macrophages (Erbilgin et al., 2018). Both in vitro and in vivo data demonstrated that Zhx2 mainly restricts the terminal maturation of NK cells. In accordance with this, *Zhx2* expression level gradually decreased during NK cell maturation, whereas mature $CD27^{low}$ NK cells displayed a minimum level of *Zhx2* (data not shown), indicating the requirement of Zhx2 suppression for NK maturation.

We have defined two pathways whereby Zhx2 controls NK cell maturation and function. One is that Zhx2 down-regulates NK cell responses to IL-15, the cytokine crucial for NK cell development and survival (Wang et al., 2019; Wang and Zhao, 2021). Deletion of *Zhx2* in NK cells resulted in increased activity of AKT and STAT5, two major signaling pathways of IL-15. Treatment with STAT5-Inh eliminated the prolonged survival and enhanced cytotoxicity in *Zhx2*-deficient NK cells. Interestingly, consistent with the role of IL-15 in regulating NK cell metabolism (Marçais et al., 2014; Wang et al., 2018) and with recently reported data showing enrichment of glycolysis-related genes in Zhx2-expressing macrophages (Wang et al., 2020), our data demonstrated that *Zhx2* loss increased the metabolic rate in NK cells and that the increased metabolic rate negatively affected NK cell survival. This highlights the importance of Zhx2 in maintaining NK cell metabolism, which should contribute to its role in controlling NK cell development and maintenance of function.

Second, we identified that the TF Zeb2 is required for Zhx2-mediated restriction of NK cell maturation. Zeb2 is expressed almost exclusively in the terminally differentiated effector and effector memory populations of $CD8^+$ T cells (Omilusik et al., 2015). This correlation of Zeb2 expression with the degree of differentiation has also been reported in NK cells (Dominguez et al., 2015). Zhx2 and Zeb2 expression inversely correlated with each other in NK cells. ATAC-seq, a ChIP assay, and dual luciferase report assays revealed that Zhx2 occupies a binding site upstream of the TSS of *Zeb2* and represses *Zeb2* transcription in NK cells. Interference of *Zeb2* destroys Zhx2-mediated repression of NK cell maturation and function. Therefore, we place Zeb2 as a downstream target of Zhx2 in the regulatory network that promotes the formation of the terminally differentiated subset of NK cells. It has been reported that T-bet is necessary for inducing *Zeb2* expression (Hu et al., 2020). We have thus analyzed T-bet expression in *Zhx2*-deficient NK cells. However, *T-bet* mRNA and protein levels were not different between $Zhx2^{+/+}$ and $Zhx2^{\Delta/\Delta}$ NK cells (data not shown), indicating that Zhx2 regulates *Zeb2* expression in a T-bet–independent manner. Moreover, because *Zeb2* has been directly or indirectly implicated in modulating IL-15–mediated survival of developing NK cells (Wang et al., 2019; Wang and Zhao, 2021), it might also link Zhx2 with IL-15 signaling. As a ubiquitous TF, Zhx2 transcriptionally regulates a variety of targets, leading to diverse functions. Here, our work proves Zeb2 as a novel target of Zhx2 in NK cells, although some other mechanisms may also exist.

The critical role of Zhx2 in restricting NK cell maturation was also observed in the tumor microenvironment. Data from TCGA showed a negative correlation of level of *ZHX2* expression in NK cells with the number of TINK cells, whereas orthotopic transplant of a liver tumor in $Zhx2^{\Delta/\Delta}$ mice had an increased number of TINK cells with enhanced maturation and fortified effector functions. Accumulation of immature NK cells has been reported in different tumors (Krneta et al., 2016). Our data strengthen the involvement of Zhx2 in the dysregulation of NK cells in the tumor microenvironment. A computational network study suggested Zhx2 as one of the most regulated TFs in myeloid cells (Espinal-Enríquez et al., 2017). Defining the key molecules causing the sustained expression of Zhx2 in TINKs or interfering *Zhx2* expression in NK cells should identify the potential targets and approaches for reversing dysfunction of TINK cells, which is definitely beneficial for tumor control.

In conclusion, our results advance the mechanistic understanding of Zhx2 control of NK cell maturation and effector functions. Deletion of *Zhx2* not only promotes IL-15–mediated NK cell activation and maturation but also allows better cell viability, resulting in better antitumor activities. Our results reveal Zhx2 as a previously unknown NK cell checkpoint and suggest that therapeutic inhibition of *Zhx2* in adoptively transferred NK cells could improve the efficacy of cancer treatments.

Materials and methods

Mice

$Ncr1^{icre}$ mice were a gift from Prof. Zhongjun Dong (Tsinghua University, Beijing, China). Cag^{cre} mice were purchased from The Jackson Laboratory. $Zhx2^{floxed}$ mice were a gift from Prof. Brett T. Spear (University of Kentucky, Lexington, KY). CD45.1 mice were kindly provided by Dr. Xiaolong Liu (Center for Excellence in Molecular Cell Science, Chinese Academy of Sciences, Shanghai, China). C57BL/6 mice (6–8 wk of age) were purchased from the Animal Research Center of Shandong University. NSG mice were purchased from Jiangsu GemPharmatech. To

generate *Ncr1*^{icre}-*Zhx2*$^{+/+}$(*Zhx2*$^{+/+}$) and *Ncr1*^{icre}-*Zhx2*$^{\Delta/\Delta}$ (*Zhx2*$^{\Delta/\Delta}$) mice, *Zhx2*$^{fl/fl}$ mice were crossed to the *Ncr1*^{icre} strain. To generate *Cag*^{cre}-*Zhx2*$^{+/+}$(*Cag*-*Zhx2*$^{+/+}$) and *Cag*^{cre}-*Zhx2*$^{\Delta/\Delta}$ (Cag-*Zhx2*$^{\Delta/\Delta}$) mice, *Zhx2*$^{fl/fl}$ mice were crossed to the *Cag*^{cre} strain. To activate Cre in *Cag*^{cre} mice, tamoxifen (T5648; Sigma-Aldrich) was injected i.p. at 2 mg for 3 d consecutively. The CD45.1$^+$ strain was crossed to the CD45.2$^+$ strain to generate the CD45.1$^+$CD45.2$^+$ strain. All mice were maintained under specific pathogen–free conditions, and experiments were performed with the Shandong University Laboratory Animal Center's approval.

Cell lines

Human NK cell line NK92 cells were cultured in α-MEM containing 12.5% FBS, 12.5% horse serum, 0.2 mM inositol, 0.1 mM 2-ME, 0.02 mM folic acid, and 100 U/ml recombinant human IL-2. The mouse cell line Yac-1 and human chronic myelocytic leukemia K562 cells were cultured in RPMI 1640 medium plus 10% FBS. Mouse melanoma B16-F10 cells, mouse hepatoma Hepa1-6 cells, human liver cancer cell lines Huh7 and HepG2, and human embryonic kidney HEK293T cells were cultured in DMEM plus 10% FBS. Cells were purchased from the American Type Culture Collection. The cell lines were authenticated in 2017, and *Mycoplasma* contamination was routinely tested.

Isolation of mononuclear cells and NK cells

For isolation of mononuclear cells from the mouse liver, tissues were harvested, teased apart, and mashed through a nylon mesh, and then the cell suspensions were centrifuged over 40% Percoll gradient medium (GE Healthcare). Mononuclear cells were obtained with fluorescent antibodies for 30 min at 4°C. NK cells were gated as CD3$^-$NK1.1$^+$CD49b$^+$ cells. NK cells applied to microarray analyses, transfer, cytotoxicity assays, immunofluorescence assays, and metabolic assays were purified by a magnetic-activated cell sorter (MACS) kit (Miltenyi Biotec). The purity of the NK cells was >90% for each assay.

FCM

Cell suspensions were surface labeled for human or mouse antibodies for 30 min at 4°C. FCM was performed on a Cytoflex S (Beckman Coulter) or Gallios flow cytometer and analyzed by FlowJo 10.6.2 or CytExpert 2.3.0.

For intracellular staining, freshly isolated cells were cultured in the medium at 37°C in a 5% CO_2 incubator and stimulated with 20 ng/ml mIL-15 (R&D Systems) for 2 h, then with brefeldin A (BioLegend) at a final concentration of 10 µg/ml for 4 h. After surface staining, cells were fixed with intracellular fixation buffer for 20 min, then permeabilized with permeabilization buffer for 10 min. Intracellular staining was performed with antibodies diluted into permeabilization buffer, and cells were fixed and permeabilized using a Fixation/Permeabilization Concentrate and Diluent Buffer Set following the manufacturer's guidelines (eBioscience). For CD107a and intracellular staining, cells were incubated with anti-NK1.1 and CD107a for 4 h at 37°C in a 5% CO_2 incubator, followed by staining for extracellular markers.

Intracellular staining for p-STAT5 (Tyr694) and p-AKT (Tyr308) was performed with the Fixation/Permeabilization Concentrate and Diluent Buffer Set according to the manufacturer's guidelines (eBioscience). Briefly, after surface staining, cells were fixed with intracellular fixation buffer for 20 min, then permeabilized with permeabilization buffer for 10 min. Intracellular phosphor staining was performed for 1 h at 4°C in the dark.

Apoptosis was analyzed by annexin V and 7-AAD double staining according to the manufacturer's instructions (BD Biosciences).

Immunoblotting

Purified NK cells or NK92 cells were lysed in radioimmunoprecipitation assay buffer (Beyotime) on ice for 30 min. The cell lysis solution was centrifuged at 12,000 *g* for 10 min, and supernatants were collected. Samples were then run on 10% Bis-Tris protein gels. Separated proteins were then transferred to polyvinylidene difluoride membranes and blocked with 5% wt/vol milk at room temperature for 2 h. Membranes were then incubated with primary antibodies in 5% wt/vol BSA in Tris-buffered saline containing 0.1% Tween-20 overnight at 4°C, then incubated with HRP-conjugated secondary antibodies (Proteintech) for 1 h at room temperature.

All antibodies for immunoblot staining are shown in Table S1.

Mixed BM chimeras

BM from sex-matched donor mice was obtained by flushing femurs and tibias. For competitive transfers, the two different BM cells were mixed at a 1:1 ratio, and a total of 1 × 10^7 BM cells were injected i.v. into recipient mice, which had been lethally irradiated with 10 Gy.

Viability and proliferation assay

Purified NK cells labeled with 5 µM CFSE were cultured with IL-2 (100 U/ml) and IL-15 (50 ng/ml) at 37°C in a 5% CO_2 incubator. After 3 d, NK cells were harvested and analyzed by FCM.

In vitro NK cell proliferation assays

Cultured NK cells from *Zhx2*$^{+/+}$ and *Zhx2*$^{\Delta/\Delta}$ mice were incubated with 0.1 nM CFSE (Beyotime) and CTV (Invitrogen), respectively. Labeled NK cells were then cocultured (1 × 10^5 of each) in vitro with IL-2 for 5 d before analysis by FCM.

Cytotoxicity assay

CFSE-labeled target cells were cocultured with purified NK cells with IL-2 (100 U/ml) at different E:T ratios (10:1, 5:1, 2.5:1) at 37°C in a 5% CO_2 incubator for 4 h. Then 7-AAD was added, and FCM identified lysed cells (CFSE$^+$7-AAD$^+$). For real-time cytotoxicity assays, the function of NK cells was monitored using a Real-Time Cell Analyzer-Multiple Plate system (PerkinElmer). This platform measures live target cells in real time. We cocultured Yac-1 cells (1 × 10^4 cells/well) as target cells and NK cells (1–10 × 10^4 cells/well) as effectors in 200 µl culture medium at 37°C with 5% CO_2. The cell index represented changes in electrical impedance and reflected the number of unkilled target cells. For real-time monitoring, the cell index was read automatically every 20 min. To determine NK cell cytotoxic activity, 2 × 10^6 CFSE-labeled Yac-1 cells were i.p. injected into WT mice

and *Zhx2* knockout mice. Cells in the peritoneal cavity were harvested, and CFSE-labeled Yac-1 cells were measured 24 h after injection. NK cells were purified using an MACS kit.

Seahorse analysis

For the extracellular assay, 2 × 10^5 purified NK cells were pretreated with 20 ng/ml IL-15 for 12 h, then seeded in a Seahorse Bioscience culture plate coated with Cell-Tak solution (Corning) in XF Base Medium Minimal DMEM (Agilent) with 10 mM glucose and 2 mM glutamine in a non-CO_2 incubator for 1 h. The basal oxygen consumption rate and maximum respiration were measured by an XF96 Seahorse Extracellular Flux Analyzer (Agilent) following the manufacturer's instructions.

Models of mouse liver cancer and NK cell transfer

Male mice 6–8 wk old were used for all experiments. In the s.c. transplanted tumor model, Hepa1-6 cells without and with purified CD3-NK1.1$^+$/Dx5$^+$ cells (ratio to Hepa1-6 cells 1:1) were inoculated in the inguinal area. The tumor sizes in each mouse were monitored using a Vernier caliper. Tumor volume was calculated by the formula $1/2ab^2$ (*a* stands for the major axis and *b* for the minor axis). For the orthotopic liver tumor model, the s.c. Hepa1-6 tumors were dissected, cut into pieces of ∼1 mm^3, and transplanted into the liver parcel of recipient mice. NSG mice were used to establish peritoneal hepatoma xenografts to assess the antitumor capacity of NK cells. To assess the killing capacity of NK cells with or without *Zhx2*, we injected human HepG2-luciferase cells (5 × 10^6) i.p. and, meanwhile, transferred NK92 cells (2 × 10^6) with LV-shNC or LV-sh*Zhx2* lentivirus infection before treatment. IL-2 (1 × 10^5 U; Jiangsu Kingsley Pharmaceuticals) was injected i.p. every 2 d to support NK cell survival in vivo. After 1 or 2 wk, for tumor imaging in vivo, luciferin was injected i.p. and imaged for 1 min using an IVIS Spectrum imaging system (PerkinElmer). NK cells were purified using an MACS kit. For the B16-F10 melanoma lung metastasis model, mice were injected with 1 × 10^6 B16-F10 melanoma cells via the caudal vein, and, 7 d later, 2 × 10^5 purified *Zhx2*$^{+/+}$ or *Zhx2*$^{Δ/Δ}$ NK cells were transferred, and IL-2 (1 × 10^5 U; Jiangsu Kingsley Pharmaceuticals) was injected i.p. every 2 d to support NK cell survival in vivo. For human HCC tumor models, we injected s.c. human HCC cell line Huh7 cells (5 × 10^6) into the groin to establish a s.c. xenograft model. After 1 wk, we transferred NK cells (2 × 10^6) with LV-shNC or LV-sh*Zhx2* lentivirus infection before treatment. IL-2 (1 × 10^5 U; Jiangsu Kingsley Pharmaceuticals) was injected i.p. every 2 d to support NK cell survival in vivo.

Analyses of gene expression

Total RNA was isolated using TRIzol reagent, and cDNA synthesis was performed using the RevertAid First Strand cDNA Synthesis Kit and random primers according to the manufacturer's instructions. Real-time qPCR and PCR were performed using SYBR Green Real-Time qPCR Master Mix (TOYOBO) and 2× Taq PCR Master Mix (Tiangen). Primer pairs for target genes are shown in Table S2.

RNA-seq analysis

The sequencing data were filtered with SOAPnuke (v1.5.2) by (1) removing reads containing sequencing adapter, (2) removing reads whose low-quality base ratio (base quality ≤5) is >20%, and (3) removing reads whose unknown base ("N" base) ratio is >5%. Afterward, clean reads were obtained and stored in FASTQ format. Raw data were uploaded into the Sequence Read Archive (accession nos. PRJNA726006, PRJNA726357). The clean reads were mapped to the reference genome using HISAT2 (v2.0.4). Bowtie2 (v2.2.5) was applied to align the clean reads to the reference coding gene set, then the expression level of gene was calculated by RSEM (v1.2.12). Essentially, differential expression analysis was performed using the PoissonDis algorithm with false discovery rate (FDR) ≤0.001 and $|\text{Log}_2\text{Ratio}| \geq 1$. To gain insight into the change of phenotype, GO (http://www.geneontology.org/) and Kyoto Encyclopedia of Gene and Genomes (https://www.kegg.jp/) enrichment analysis of annotated differently expressed genes was performed by phyper (https://stat.ethz.ch/R-manual/R-devel/library/stats/html/Hypergeometric.html) on the basis of a hypergeometric test. The significance levels of terms and pathways were corrected by Q value with a rigorous threshold ($Q \leq 0.05$) by the Bonferroni correction.

Statistical analyses

Statistical significance was determined using Prism 8.3.0 (GraphPad Software). Two-tailed unpaired or paired Student's *t* tests between two groups and two-way ANOVA across multiple groups were used to determine significance. The difference in overall survival was tested using log-rank tests. Data are presented as mean ± SEM. Statistical significance was reported as *, $P < 0.05$; **, $P < 0.01$; ***, $P < 0.001$; and n.s., no significance.

Online supplemental material

Fig. S1 shows Zhx2 cell and subcell profiling. Fig. S2 explains how Zhx2 inhibits NK cell functions. Fig. S3 illustrates how Zhx2 weakens IL-15–promoted NK cell function. Fig. S4 shows distinct transcriptome profiles and ATAC peaks in *Zhx2*-deficient NK cells. Fig. S5 shows that Zhx2 inhibits NK cell maturation and function in the tumor microenvironment. Table S1 lists antibodies used for FCM and Western blot analysis. Table S2 lists sequences of primers used for RT-qPCR.

Data availability

The RNA-seq data and ATAC-seq data in this publication have been deposited in the National Center for Biotechnology Information Sequence Read Archive and are accessible through accession nos. PRJNA726006 and PRJNA726357.

Acknowledgments

The graphical abstract was prepared using BioRender software.

This study was supported in part by the National Natural Science Foundation of China (key program 81830017 and nos. 81902433, 81902051), the National Outstanding Youth Science Fund Project of National Natural Science Foundation of China (81425012), the Taishan Scholar Foundation of Shandong Province (tspd20181201), the Collaborative Innovation Center of Technology and Equipment for Biological Diagnosis and Therapy in Universities of Shandong, the Key Research and Development

Program of Shandong (2018YFJH0503), and the National Key Research and Development Program (2018YFE0126500).

Author contributions: C. Ma and S. Tan formulated the study concept. C. Ma and S. Tan designed the studies. S. Tan, X. Guo, M. Li, T. Wang, Z. Wang, Z. Wu, and C. Li performed the experiments. S. Tan, X. Guo, and C. Ma analyzed the results. X. Liang, L. Gao, N. Li, and C. Ma interpreted the results. S. Tan, X. Liang, L. Gao, N. Li, and C. Ma wrote and edited the manuscript.

Disclosures: The authors declare no competing interests exist.

Submitted: 2 January 2021
Revised: 5 May 2021
Accepted: 17 June 2021

References

Aran, D., Z. Hu, and A.J. Butte. 2017. xCell: digitally portraying the tissue cellular heterogeneity landscape. *Genome Biol.* 18:220. https://doi.org/10.1186/s13059-017-1349-1

Barton, K., N. Muthusamy, C. Fischer, C.N. Ting, T.L. Walunas, L.L. Lanier, and J.M. Leiden. 1998. The Ets-1 transcription factor is required for the development of natural killer cells in mice. *Immunity.* 9:555–563. https://doi.org/10.1016/S1074-7613(00)80638-X

Brillantes, M., and A.M. Beaulieu. 2019. Transcriptional control of natural killer cell differentiation. *Immunology.* 156:111–119. https://doi.org/10.1111/imm.13017

Chiossone, L., J. Chaix, N. Fuseri, C. Roth, E. Vivier, and T. Walzer. 2009. Maturation of mouse NK cells is a 4-stage developmental program. *Blood.* 113:5488–5496. https://doi.org/10.1182/blood-2008-10-187179

Constantinides, M.G., B.D. McDonald, P.A. Verhoef, and A. Bendelac. 2014. A committed precursor to innate lymphoid cells. *Nature.* 508:397–401. https://doi.org/10.1038/nature13047

Delconte, R.B., W. Shi, P. Sathe, T. Ushiki, C. Seillet, M. Minnich, T.B. Kolesnik, L.C. Rankin, L.A. Mielke, J.G. Zhang, et al. 2016. The helix-loop-helix protein ID2 governs NK cell fate by tuning their sensitivity to interleukin-15. *Immunity.* 44:103–115. https://doi.org/10.1016/j.immuni.2015.12.007

Dogra, P., C. Rancan, W. Ma, M. Toth, T. Senda, D.J. Carpenter, M. Kubota, R. Matsumoto, P. Thapa, P.A. Szabo, et al. 2020. Tissue determinants of human NK cell development, function, and residence. *Cell.* 180:749–763.e13. https://doi.org/10.1016/j.cell.2020.01.022

Dominguez, C.X., R.A. Amezquita, T. Guan, H.D. Marshall, N.S. Joshi, S.H. Kleinstein, and S.M. Kaech. 2015. The transcription factors ZEB2 and T-bet cooperate to program cytotoxic T cell terminal differentiation in response to LCMV viral infection. *J. Exp. Med.* 212:2041–2056. https://doi.org/10.1084/jem.20150186

Erbilgin, A., M.M. Seldin, X. Wu, M. Mehrabian, Z. Zhou, H. Qi, K.S. Dabirian, R.R. Sevag Packard, W. Hsieh, S.J. Bensinger, et al. 2018. Transcription factor Zhx2 deficiency reduces atherosclerosis and promotes macrophage apoptosis in mice. *Arterioscler. Thromb. Vasc. Biol.* 38:2016–2027. https://doi.org/10.1161/ATVBAHA.118.311266

Espinal-Enríquez, J., D. González-Terán, and E. Hernández-Lemus. 2017. The transcriptional network structure of a myeloid cell: a computational approach. *Int. J. Genomics.* 2017:4858173. https://doi.org/10.1155/2017/4858173

Gordon, S.M., J. Chaix, L.J. Rupp, J. Wu, S. Madera, J.C. Sun, T. Lindsten, and S.L. Reiner. 2012. The transcription factors T-bet and Eomes control key checkpoints of natural killer cell maturation. *Immunity.* 36:55–67. https://doi.org/10.1016/j.immuni.2011.11.016

Guillerey, C., N.D. Huntington, and M.J. Smyth. 2016. Targeting natural killer cells in cancer immunotherapy. *Nat. Immunol.* 17:1025–1036. https://doi.org/10.1038/ni.3518

Hu, M., Y. Lu, Y. Qi, Z. Zhang, S. Wang, Y. Xu, F. Chen, Y. Tang, S. Chen, M. Chen, et al. 2020. SRC-3 functions as a coactivator of T-bet by regulating the maturation and antitumor activity of natural killer cells. *Cancer Immunol. Res.* 8:1150–1162. https://doi.org/10.1158/2326-6066.CIR-20-0181

Huntington, N.D., H. Tabarias, K. Fairfax, J. Brady, Y. Hayakawa, M.A. Degli-Esposti, M.J. Smyth, D.M. Tarlinton, and S.L. Nutt. 2007a. NK cell maturation and peripheral homeostasis is associated with KLRG1 up-regulation. *J. Immunol.* 178:4764–4770. https://doi.org/10.4049/jimmunol.178.8.4764

Huntington, N.D., C.A. Vosshenrich, and J.P. Di Santo. 2007b. Developmental pathways that generate natural-killer-cell diversity in mice and humans. *Nat. Rev. Immunol.* 7:703–714. https://doi.org/10.1038/nri2154

Hystad, M.E., J.H. Myklebust, T.H. Bø, E.A. Sivertsen, E. Rian, L. Forfang, E. Munthe, A. Rosenwald, M. Chiorazzi, I. Jonassen, et al. 2007. Characterization of early stages of human B cell development by gene expression profiling. *J. Immunol.* 179:3662–3671. https://doi.org/10.4049/jimmunol.179.6.3662

Jacobs, R., G. Hintzen, A. Kemper, K. Beul, S. Kempf, G. Behrens, K.W. Sykora, and R.E. Schmidt. 2001. CD56^{bright} cells differ in their KIR repertoire and cytotoxic features from CD56^{dim} NK cells. *Eur. J. Immunol.* 31:3121–3127. https://doi.org/10.1002/1521-4141(2001010)31:10<3121::AID-IMMU3121>3.0.CO;2-4

Juen, L., M. Brachet-Botineau, C. Parmenon, J. Bourgeais, O. Hérault, F. Gouilleux, M.C. Viaud-Massuard, and G. Prié. 2017. New inhibitor targeting signal transducer and activator of transcription 5 (STAT5) signaling in myeloid leukemias. *J. Med. Chem.* 60:6119–6136. https://doi.org/10.1021/acs.jmedchem.7b00369

Kim, S., K. Iizuka, H.S. Kang, A. Dokun, A.R. French, S. Greco, and W.M. Yokoyama. 2002. In vivo developmental stages in murine natural killer cell maturation. *Nat. Immunol.* 3:523–528. https://doi.org/10.1038/ni796

Kobayashi, T., and S.R. Mattarollo. 2019. Natural killer cell metabolism. *Mol. Immunol.* 115:3–11. https://doi.org/10.1016/j.molimm.2017.11.021

Krneta, T., A. Gillgrass, M. Chew, and A.A. Ashkar. 2016. The breast tumor microenvironment alters the phenotype and function of natural killer cells. *Cell. Mol. Immunol.* 13:628–639. https://doi.org/10.1038/cmi.2015.42

Lin, J.X., N. Du, P. Li, M. Kazemian, T. Gebregiorgis, R. Spolski, and W.J. Leonard. 2017. Critical functions for STAT5 tetramers in the maturation and survival of natural killer cells. *Nat. Commun.* 8:1320. https://doi.org/10.1038/s41467-017-01477-5

Liu, Y., D. Ma, and C. Ji. 2015. Zinc fingers and homeoboxes family in human diseases. *Cancer Gene Ther.* 22:223–226. https://doi.org/10.1038/cgt.2015.16

Mamessier, E., A. Sylvain, M.L. Thibult, G. Houvenaeghel, J. Jacquemier, R. Castellano, A. Gonçalves, P. André, F. Romagné, G. Thibault, et al. 2011. Human breast cancer cells enhance self tolerance by promoting evasion from NK cell antitumor immunity. *J. Clin. Invest.* 121:3609–3622. https://doi.org/10.1172/JCI45816

Marçais, A., J. Cherfils-Vicini, C. Viant, S. Degouve, S. Viel, A. Fenis, J. Rabilloud, K. Mayol, A. Tavares, J. Bienvenu, et al. 2014. The metabolic checkpoint kinase mTOR is essential for IL-15 signaling during the development and activation of NK cells. *Nat. Immunol.* 15:749–757. https://doi.org/10.1038/ni.2936

Meinhardt, K., I. Kroeger, R. Bauer, F. Ganss, I. Ovsiy, J. Rothamer, M. Büttner, I. Atreya, M. Waldner, M. Bittrich, et al. 2015. Identification and characterization of the specific murine NK cell subset supporting graft-*versus*-leukemia- and reducing graft-*versus*-host-effects. *OncoImmunology.* 4:e981483. https://doi.org/10.4161/2162402X.2014.981483

Mishra, A., L. Sullivan, and M.A. Caligiuri. 2014. Molecular pathways: interleukin-15 signaling in health and in cancer. *Clin. Cancer Res.* 20:2044–2050. https://doi.org/10.1158/1078-0432.CCR-12-3603

Nagel, S., C. Meyer, M. Kaufmann, H.G. Drexler, and R.A. MacLeod. 2014. Deregulated FOX genes in Hodgkin lymphoma. *Genes Chromosomes Cancer.* 53:917–933. https://doi.org/10.1002/gcc.22204

Nagel, S., S. Ehrentraut, C. Meyer, M. Kaufmann, H.G. Drexler, and R.A. MacLeod. 2015. Aberrantly expressed OTX homeobox genes deregulate B-cell differentiation in Hodgkin lymphoma. *PLoS One.* 10:e0138416. https://doi.org/10.1371/journal.pone.0138416

Omilusik, K.D., J.A. Best, B. Yu, S. Goossens, A. Weidemann, J.V. Nguyen, E. Seuntjens, A. Stryjewska, C. Zweier, R. Roychoudhuri, et al. 2015. Transcriptional repressor ZEB2 promotes terminal differentiation of CD8^{+} effector and memory T cell populations during infection. *J. Exp. Med.* 212:2027–2039. https://doi.org/10.1084/jem.20150194

Platonova, S., J. Cherfils-Vicini, D. Damotte, L. Crozet, V. Vieillard, P. Validire, P. André, M.C. Dieu-Nosjean, M. Alifano, J.F. Régnard, et al. 2011. Profound coordinated alterations of intratumoral NK cell phenotype and function in lung carcinoma. *Cancer Res.* 71:5412–5422. https://doi.org/10.1158/0008-5472.CAN-10-4179

Richards, J.O., X. Chang, B.W. Blaser, M.A. Caligiuri, P. Zheng, and Y. Liu. 2006. Tumor growth impedes natural-killer-cell maturation in the bone

marrow. *Blood.* 108:246–252. https://doi.org/10.1182/blood-2005-11-4535

Sconocchia, G., R. Arriga, L. Tornillo, L. Terracciano, S. Ferrone, and G.C. Spagnoli. 2012. Melanoma cells inhibit NK cell functions. *Cancer Res.* 72: 5428–5429, author reply: 5430. https://doi.org/10.1158/0008-5472.CAN-12-1181

Seillet, C., L.C. Rankin, J.R. Groom, L.A. Mielke, J. Tellier, M. Chopin, N.D. Huntington, G.T. Belz, and S. Carotta. 2014. Nfil3 is required for the development of all innate lymphoid cell subsets. *J. Exp. Med.* 211: 1733–1740. https://doi.org/10.1084/jem.20140145

Shen, H., F. Luan, H. Liu, L. Gao, X. Liang, L. Zhang, W. Sun, and C. Ma. 2008. ZHX2 is a repressor of alpha-fetoprotein expression in human hepatoma cell lines. *J. Cell. Mol. Med.* 12(6b, 6B):2772–2780. https://doi.org/10.1111/j.1582-4934.2008.00233.x

Tang, Y., C. Peitzsch, H.N. Charoudeh, M. Cheng, P. Chaves, S.E. Jacobsen, and E. Sitnicka. 2012. Emergence of NK-cell progenitors and functionally competent NK-cell lineage subsets in the early mouse embryo. *Blood.* 120:63–75. https://doi.org/10.1182/blood-2011-02-337980

Taveirne, S., S. Wahlen, W. Van Loocke, L. Kiekens, E. Persyn, E. Van Ammel, K. De Mulder, J. Roels, L. Tilleman, M. Aumercier, et al. 2020. The transcription factor ETS1 is an important regulator of human NK cell development and terminal differentiation. *Blood.* 136:288–298. https://doi.org/10.1182/blood.2020005204

van Helden, M.J., S. Goossens, C. Daussy, A.L. Mathieu, F. Faure, A. Marçais, N. Vandamme, N. Farla, K. Mayol, S. Viel, et al. 2015. Terminal NK cell maturation is controlled by concerted actions of T-bet and Zeb2 and is essential for melanoma rejection. *J. Exp. Med.* 212:2015–2025. https://doi.org/10.1084/jem.20150809

Vargas-Hernández, A., A. Witalisz-Siepracka, M. Prchal-Murphy, K. Klein, S. Mahapatra, W. Al-Herz, E.M. Mace, A.F. Carisey, J.S. Orange, V. Sexl, and L.R. Forbes. 2020. Human signal transducer and activator of transcription 5b (STAT5b) mutation causes dysregulated human natural killer cell maturation and impaired lytic function. *J. Allergy Clin. Immunol.* 145:345–357.e9. https://doi.org/10.1016/j.jaci.2019.09.016

Vivier, E., E. Tomasello, M. Baratin, T. Walzer, and S. Ugolini. 2008. Functions of natural killer cells. *Nat. Immunol.* 9:503–510. https://doi.org/10.1038/ni1582

Vong, Q.P., W.H. Leung, J. Houston, Y. Li, B. Rooney, M. Holladay, R.A. Oostendorp, and W. Leung. 2014. TOX2 regulates human natural killer cell development by controlling T-BET expression. *Blood.* 124:3905–3913. https://doi.org/10.1182/blood-2014-06-582965

Waldmann, T.A. 2015. The shared and contrasting roles of IL2 and IL15 in the life and death of normal and neoplastic lymphocytes: implications for cancer therapy. *Cancer Immunol. Res.* 3:219–227. https://doi.org/10.1158/2326-6066.CIR-15-0009

Wang, X., X.-Y. Zhao, et al. 2021. Transcription Factors Associated With IL-15 Cytokine Signaling During NK Cell Development. *Front. Immunol.* 12: 610789. https://doi.org/10.3389/fimmu.2021.610789

Wang, F., M. Meng, B. Mo, Y. Yang, Y. Ji, P. Huang, W. Lai, X. Pan, T. You, H. Luo, et al. 2018. Crosstalks between mTORC1 and mTORC2 variagate cytokine signaling to control NK maturation and effector function. *Nat. Commun.* 9:4874. https://doi.org/10.1038/s41467-018-07277-9

Wang, Y., Y. Zhang, P. Yi, W. Dong, A.P. Nalin, J. Zhang, Z. Zhu, L. Chen, D.M. Benson, B.L. Mundy-Bosse, et al. 2019. The IL-15-AKT-XBP1s signaling pathway contributes to effector functions and survival in human NK cells. *Nat. Immunol.* 20:10–17. https://doi.org/10.1038/s41590-018-0265-1

Wang, Z., L. Kong, S. Tan, Y. Zhang, X. Song, T. Wang, Q. Lin, Z. Wu, P. Xiang, C. Li, et al. 2020. Zhx2 accelerates sepsis by promoting macrophage glycolysis via Pfkfb3. *J. Immunol.* 204:2232–2241. https://doi.org/10.4049/jimmunol.1901246

Wang, Y., Y. Zhang, P. Yi, W. Dong, A.P. Nalin, J. Zhang, Z. Zhu, L. Chen, D.M. Benson, B.L. Mundy-Bosse, et al. 2019. The IL-15-AKT-XBP1s signaling pathway contributes to effector functions and survival in human NK cells. *Nat. Immunol.* 20:10–17. https://doi.org/10.1038/s41590-018-0265-1

White, M.J., C.M. Beaver, M.R. Goodier, C. Bottomley, C.M. Nielsen, A.F. Wolf, L. Boldrin, C. Whitmore, J. Morgan, D.J. Pearce, and E.M. Riley. 2017. Calorie restriction attenuates terminal differentiation of immune cells. *Front. Immunol.* 7:667. https://doi.org/10.3389/fimmu.2016.00667

Wu, Z., H. Ma, L. Wang, X. Song, J. Zhang, W. Liu, Y. Ge, Y. Sun, X. Yu, Z. Wang, et al. 2020a. Tumor suppressor ZHX2 inhibits NAFLD-HCC progression via blocking LPL-mediated lipid uptake. *Cell Death Differ.* 27:1693–1708. https://doi.org/10.1038/s41418-019-0453-z

Wu, Z., H. Ma, L. Wang, X. Song, J. Zhang, W. Liu, Y. Ge, Y. Sun, X. Yu, Z. Wang, et al. 2020b. Tumor suppressor ZHX2 inhibits NAFLD-HCC progression via blocking LPL-mediated lipid uptake. *Cell Death Differ.* 27:1693–1708. https://doi.org/10.1038/s41418-019-0453-z

You, Y., F. Bai, H. Li, Y. Ma, L. Yao, J. Hu, and Y. Tian. 2020. Prognostic value and therapeutic implications of ZHX family member expression in human gastric cancer. *Am. J. Transl. Res.* 12:3376–3388.

Yue, X., Z. Zhang, X. Liang, L. Gao, X. Zhang, D. Zhao, X. Liu, H. Ma, M. Guo, B.T. Spear, et al. 2012. Zinc fingers and homeoboxes 2 inhibits hepatocellular carcinoma cell proliferation and represses expression of Cyclins A and E. *Gastroenterology.* 142:1559–70.e2. https://doi.org/10.1053/j.gastro.2012.02.049

Zhao, J., S. Zhang, Y. Liu, X. He, M. Qu, G. Xu, H. Wang, M. Huang, J. Pan, Z. Liu, et al. 2020. Single-cell RNA sequencing reveals the heterogeneity of liver-resident immune cells in human. *Cell Discov.* 6:22. https://doi.org/10.1038/s41421-020-0157-z

JEM

Supplemental material

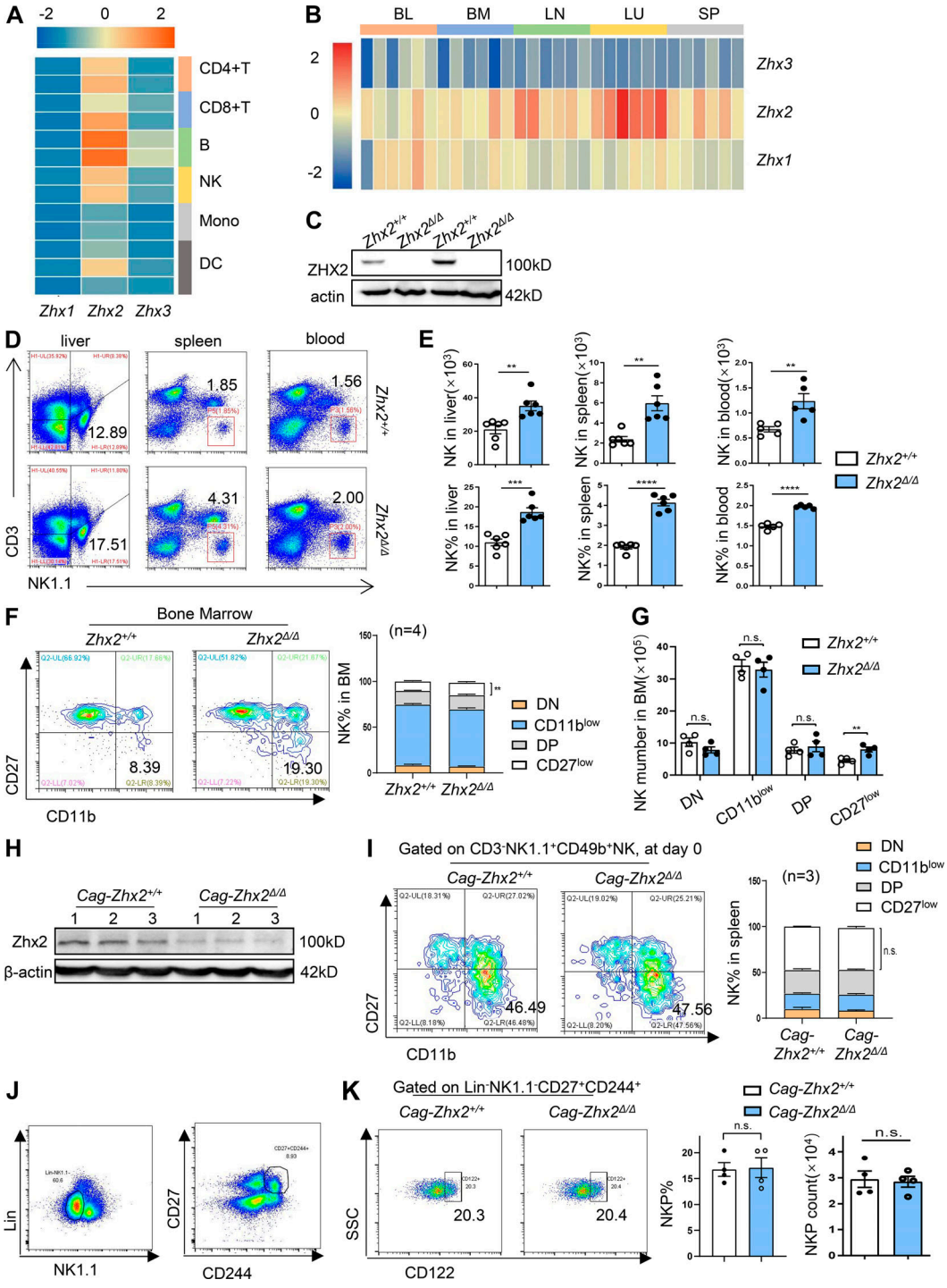

Figure S1. **Zhx2 cell and subcell profiling. (A)** Specific expression of *ZHX1/2/3* in different immune cells. RNA-seq data are adopted from Gene Expression Omnibus accession no. GSE125188. **(B)** Expression of *Zhx1/2/3* in NK cells isolated from indicated tissues. RNA-seq data are adopted from Gene Expression Omnibus accession no. GSE133383.BL, blood; LU, lung; SP, spleen. **(C)** Western blot detecting Zhx2 expression in purified splenic NK cells from *Zhx2*$^{+/+}$ and *Zhx2*$^{Δ/Δ}$ mice. Actin was used as the loading control. **(D and E)** FACS plots and bar graphs represent percentages and absolute numbers of CD3^{-}NK1.1^{+} NK cells in the liver, spleen, and blood from *Zhx2*$^{+/+}$ and *Zhx2*$^{Δ/Δ}$ mice (representative of at least three independent experiments). **(F)** FACS plots and bar graphs depict NK cell subsets determined by expression of CD11b/CD27 in BM from *Zhx2*$^{+/+}$ and *Zhx2*$^{Δ/Δ}$ mice (representative of three independent experiments). **(G)** NK cell counts in the indicated subsets from BM of *Zhx2*$^{+/+}$ and *Zhx2*$^{Δ/Δ}$ mice (representative of three independent experiments). DN, double negative. **(H)** Western blot detecting Zhx2 expression in purified splenic NK cells from *Cag-Zhx2*$^{+/+}$ and *Cag-Zhx2*$^{Δ/Δ}$ mice. Actin was used as the loading control. **(I)** FACS plots and bar graphs depict NK cell subsets determined by expression of CD11b/CD27 in the spleen from Cag-*Zhx2*$^{+/+}$ and Cag-*Zhx2*$^{Δ/Δ}$ mice at day 0 before in vitro culture (representative of three independent experiments). **(J)** FCM analysis of NKP cells marked as Lin^{-}CD27^{+}CD244^{+}CD122^{+}NK1.1^{-}. **(K)** NKP cell percentage and number in the spleen are shown (representative of two independent experiments). Each dot represents data from an individual mouse, and error bars represent SEM per group in one experiment. Data were analyzed using Student's *t* test (two-tailed paired *t* test) in E–G, I, and K. *, P < 0.05; **, P < 0.0001; ***, P < 0.001; ****, P < 0.0001.

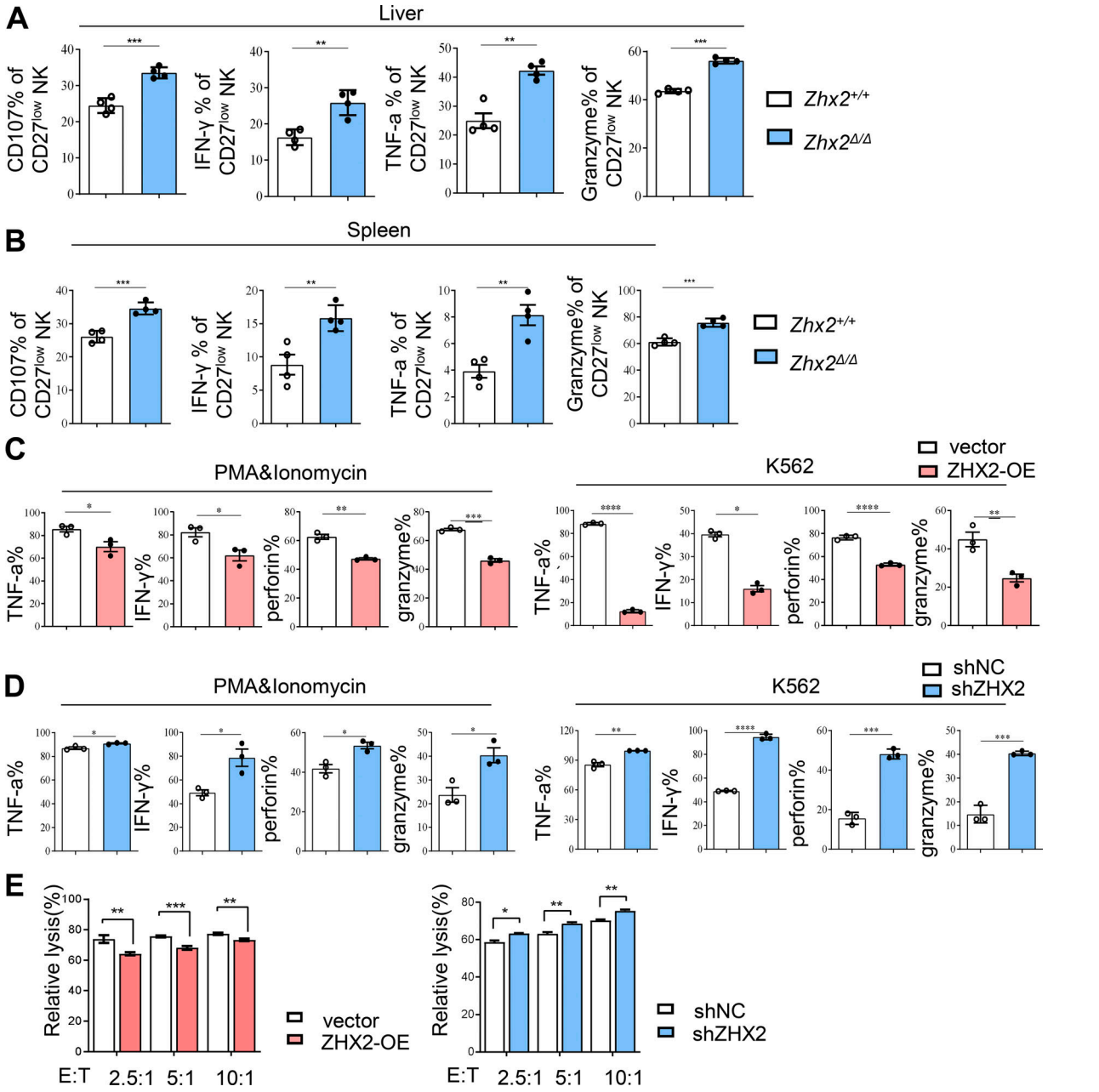

Figure S2. **Zhx2 inhibits NK cell functions. (A)** Percentage of indicated effector molecules assessed with FCM in anti-NK1.1–stimulated CD27⁻CD11b⁺ liver NK cells. Cells were pregated on CD3⁻NK1.1⁺ subsets (representative of three independent experiments). **(B)** Percentage of indicated effector molecules assessed with FCM in anti-NK1.1–stimulated CD27⁻CD11b⁺ spleen NK cells. Cells were pregated on CD3⁻NK1.1⁺ subsets (representative of three independent experiments). **(C)** IFN-γ, TNF-α, perforin, and granzyme production in NK92 cells transfected with *ZHX2* overexpression (*ZHX2*-OE) plasmid or empty vector (control; representative of three independent experiments). **(D)** IFN-γ, TNF-α, perforin, and granzyme production in NK92 cells infected with *ZHX2* shRNA expressing lentivirus (sh*ZHX2*) or control shRNA lentivirus (representative of three independent experiments). **(E)** NK92 cells with indicated treatment were cocultured with CFSE-labeled K562 cells for 6 h. FCM assay was used to detect 7-AAD staining in K562 cells (representative of three independent experiments). Each symbol represents data from an individual sample, and error bars represent SEM per group in one experiment. Data were analyzed using Student's *t* test (two-tailed paired *t* test). *, P < 0.05; **, P < 0.0001; ***, P < 0.001; ****, P < 0.0001.

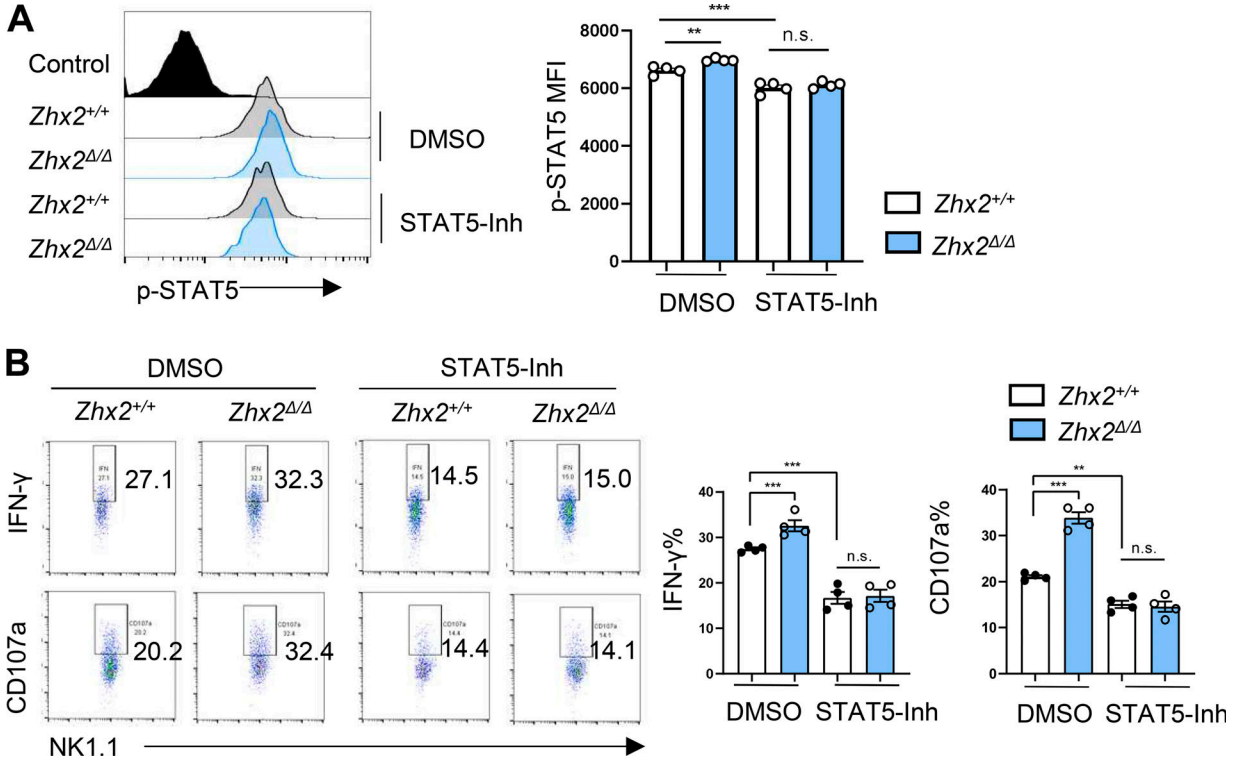

Figure S3. **Zhx2 weakens IL-15–promoted NK cell function.** Splenic NK cells from *Zhx2*$^{+/+}$ and *Zhx2*$^{\Delta/\Delta}$ mice were stimulated with PMA with or without the presence of STAT5-Inh (10 mM; representative of two independent experiments). **(A and B)** FACS plots and graphs show the mean fluorescence intensity of AKT phosphorylation (A) and percentage of CD107a- and IFN-γ–expressing NK cells (B). Error bars represent SEM per group in one experiment. Data were analyzed using Student's *t* test (two-tailed paired *t* test). **, P < 0.0001; ***, P < 0.001.

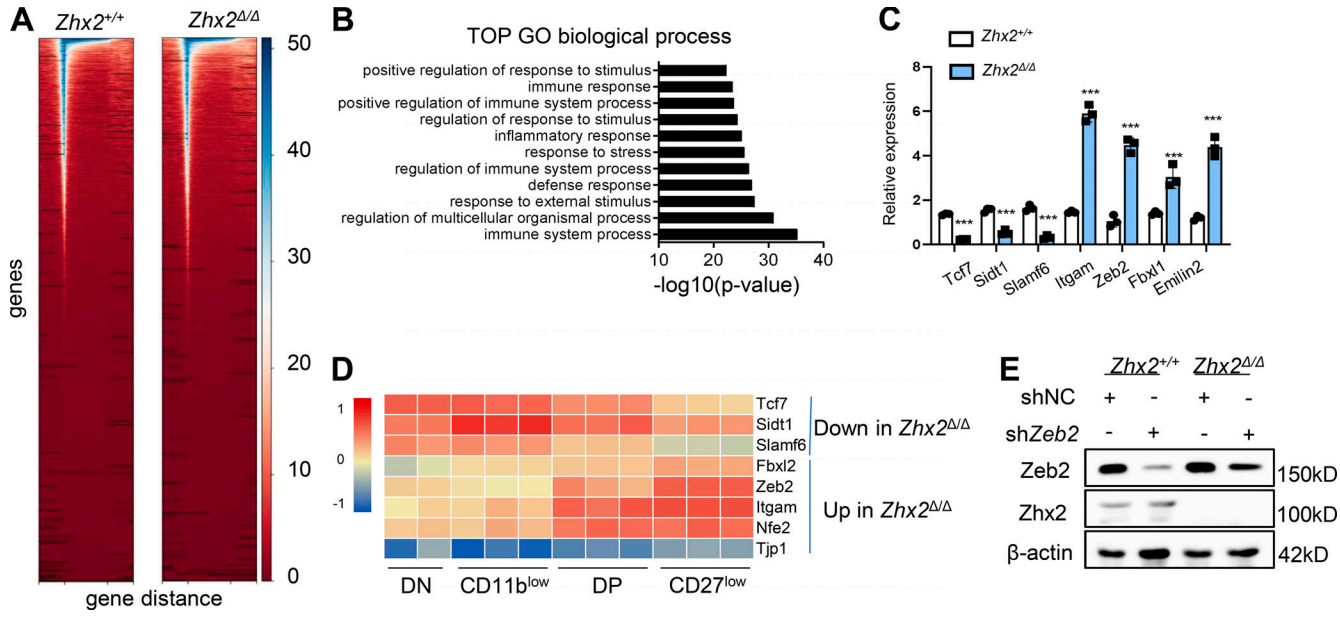

Figure S4. **Distinct transcriptomic profiles and ATAC peaks in *Zhx2*-deficient NK cells. (A)** Chromatin accessibility of *Zhx2*$^{+/+}$ and *Zhx2*$^{\Delta/\Delta}$ NK cells accessed by ATAC-seq. Each row represents one peak (differentially accessible between *Zhx2*$^{+/+}$ and *Zhx2*$^{\Delta/\Delta}$ NK cells; FDR ≤ 0.05). **(B)** GO enrichment analysis is illustrated. The analysis was performed on the differentially expressed genes by likelihood ratio tests. P ≤ 0.05. **(C)** Real-time qPCR analysis of indicated gene expression in purified splenic NK cells from *Zhx2*$^{+/+}$ and *Zhx2*$^{\Delta/\Delta}$ mice (representative of two independent experiments). **(D)** Specific expression of the indicated genes in NK cell development. RNA-seq data are adopted from Gene Expression Omnibus accession no. GSE45842. **(E)** Western blot analysis of the protein expression of Zhx2 and Zeb2 in the indicated NK cells. Error bars represent SEM per group in one experiment. Data were analyzed using Student's *t* test (two-tailed paired *t* test). ***, P < 0.001.

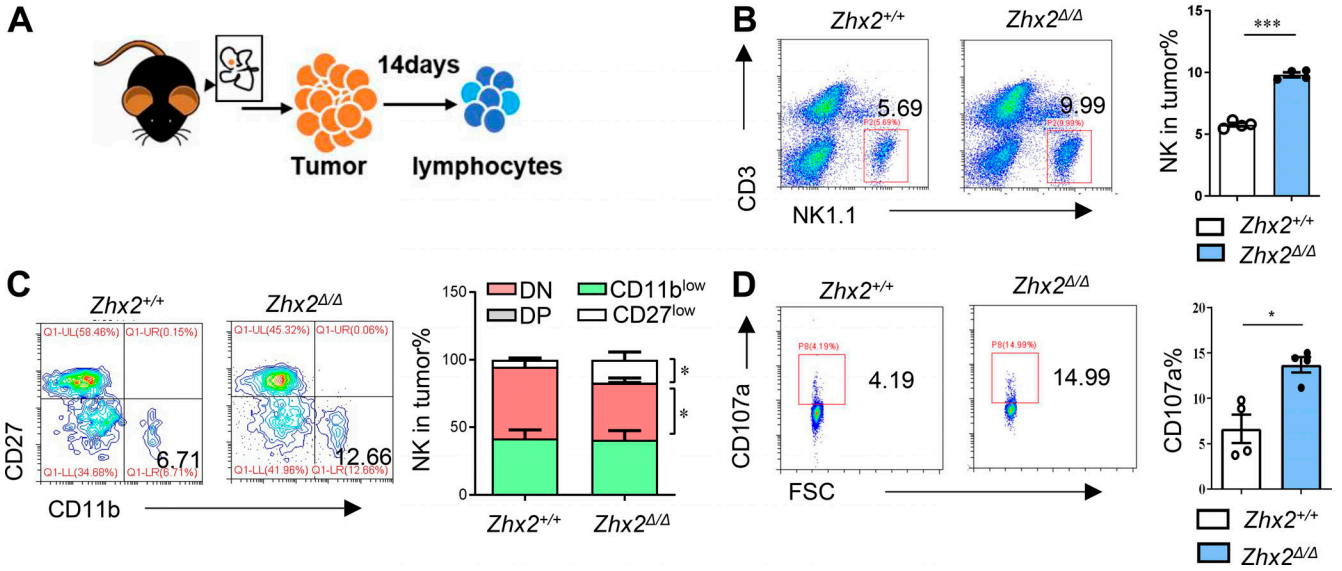

Figure S5. **Zhx2 inhibits NK cell maturation and function in the tumor microenvironment. (A–D)** A murine model of orthotopically HCC was created, and NK cells were harvested for FCM analyses (representative of two independent experiments). **(A)** Scheme of the experimental design. **(B)** FCM measurement of HCC TINK cell percentage. **(C)** Frequency of mature NK cells in the tumor microenvironment. Cells were pregated on $CD3^{-}NK1.1^{+}$ subsets. **(D)** CD107a production of TINK cells from $Zhx2^{+/+}$ and $Zhx2^{\Delta/\Delta}$ mice. Error bars represent SEM per group in one experiment. Data were analyzed using Student's *t* test (two-tailed paired *t* test). FSC, forward scatter. *, $P < 0.05$; ***, $P < 0.001$.

Table S1 lists antibodies used for FCM and Western blot analysis. Table S2 lists sequences of primers used for RT-qPCR.